

Kinetic description of charmonium production in high-energy nuclear collisions

Alberto Polleri^{a,b}, Thorsten Renk^a, Roland Schneider^a, and Wolfram Weise^{a,b}
^a*Physik Department, Technische Universität München, D-85747 Garching, Germany*
^b*ECT*, Villa Tambosi, I-38050 Villazzano (Trento), Italy*

We study the evolution of charmonia as they collide with the constituents of the fireball produced in high-energy nucleus-nucleus collisions. The latter evolves in a manner controlled by the equation of state as given by lattice QCD, and is constructed in such a way that the observed hadronic spectra are correctly reproduced. A kinetic description of charmonium interactions with both quark-gluon and hadronic degrees of freedom allows to study in detail the evolution in different regimes, controlled by collision energy, kinematics and geometry. The data collected at the CERN-SPS accelerator are well described and new estimates for J/ψ production at BNL-RHIC are presented.

PACS numbers: 25.75.-q, 25.75.Nq, 24.85.+p, 14.40.Gx

I. INTRODUCTION

The very first suggestion to study J/ψ production and suppression in heavy-ion collisions [1] was based on a two-fold observation: First, the energy density accumulated in such collisions is expected to be high enough that the medium formed in the collision presumably undergoes a transition from hadronic matter to a quark-gluon plasma (QGP). Second, J/ψ is bound essentially by the confinement force which, when screened in the QGP, loses its binding character. Produced J/ψ s dissolve and their charm quarks end up in pairs of D mesons. The expectation is therefore that the J/ψ production cross section is suppressed in a hot and dense environment as compared with extrapolations from proton-proton (pp) collisions.

Indeed, lattice simulations [2] indicate that QCD with (2+1) flavors undergoes a transition at a temperature of about 170 MeV [3] from a confined hadronic phase to a phase where quarks and gluons constitute the relevant active degrees of freedom. The possible existence of this new state of matter has raised enormous interest, and the search for experimental evidence of its creation continues since about 20 years. Yet there is still no unambiguous proof that the QGP has been produced in the laboratory. A primary reason for this is that any QGP signature, including J/ψ suppression, is folded with the time evolution of the fireball created in such a collision. Moreover, the evolution continues after the supposedly produced plasma undergoes a transition from partonic to hadronic degrees of freedom. Any information on the early stage is then hidden behind signals from the hadronic phase. Finally, the most important uncertainty is perhaps the poor knowledge of the process of thermalization. The particularly interesting case of J/ψ suppression is thus subject of a vigorous experimental search and theoretical debate. The first systematic signs of suppression [4] were later on explained by more conventional mechanisms [5], already present in proton-nucleus (pA) reactions. Only with the beginning of the experimental search using $Pb+Pb$ collisions the first signals of anomalous suppression, beyond extrapolations from pA collisions, were seen [6].

While much phenomenology has been developed in or-

der to explain the latest SPS data [7], it is still debated whether or not anomalous suppression can be attributed to QGP formation. In fact, realistic models can be constructed which incorporate well known nuclear effects such as initial state gluon radiation [8], color excitation [9], initial state parton energy loss [10] and coherence effects [11]. All of these can potentially account for the observed data because they provide the necessary non-linear dependence on the number of participating particles which becomes significant only when going beyond pA collisions.

In view of the uncertainties inherent in the construction of models which consider such effects, we attempt an approach to the problem which maximizes the number of independent physical constraints. The usual strategy is to attribute the missing suppression to medium effects, exclusively designed to handle the J/ψ case alone. For this procedure to be conclusive one needs a very reliable baseline for the description of the production process. Here we adopt a different and novel perspective and make use of the knowledge of the medium evolution as inferred by a variety of other observables. We then explore whether the same description is consistent with the observed J/ψ measurements. We stress that this is possible because the specific time evolution of the medium is not constructed or fitted in order to reproduce the J/ψ suppression effect, but it is constrained beforehand by other independent data.

We treat charmonium production in nucleus-nucleus (AB) collisions as a two-step process, factorizing direct production from the subsequent evolution in the medium. The first part includes the conventional description [13] of nuclear effects within the Glauber model framework, with values of the absorption cross section either extrapolated from the suppression observed experimentally already in pA collisions, or fitted to reproduce the results of more sophisticated computations [11, 12]. The second part is a description within kinetic theory of the interaction of J/ψ s with the different degrees of freedom that populate the evolving medium at different times. In this framework interactions are realized by cross sections, while the evolution of the medium itself is constrained by an independent description of hadronic spectra. With

this procedure we are able to specify the nature of the medium and to follow the detailed time evolution of J/ψ mesons.

It might seem natural at this stage to also incorporate the mentioned Debye screening of the inter-quark potential, for example by assuming complete J/ψ dissolution above a certain temperature [14, 15]. However, it is not clear what an all-embracing description of the interaction of the J/ψ with the medium should be. Screening arises from the interaction of the virtual gluons that bind the J/ψ with the gluons of the environment. Such a process can also be viewed as scattering of the J/ψ , that fluctuates into a $c\bar{c}$ pair and non-perturbative multi-gluon exchanges, off the thermalized gluons [16]. Taking into account both screening and kinetic scattering can amount to a certain degree to double counting. Disentangling these effects even qualitatively, however, is a highly non-trivial task which requires a dedicated analysis. At this stage, we can say that screening, as inferred from lattice QCD, is a purely static concept. Since J/ψ s are not produced at rest with respect to the medium, a kinetic approach seems to be appropriate within the present context. Obviously, a more rigorous treatment of this question is required in the future.

The paper is structured in four sections. First, the initial conditions for the solution of the kinetic equation are discussed. We provide a simple extension of the parton model prescription for the $pp \rightarrow c\bar{c}X$ process, scaling the open charm production cross section with the average number of collisions. At the same time charmonium production is computed treating nuclear suppression as effective Glauber absorption. We take into account the role of excited charmonium states ψ' and χ which contribute sequentially to J/ψ production. We will often denote charmonia generically by Ψ as a shorthand notation.

In the following section a thorough description of the produced medium is given. This medium is assumed to thermalize and then described within a thermodynamically consistent quasi-particle picture [17], incorporating important aspects of confinement. This approach treats quarks and gluons as massive thermal quasi-particles, with their properties determined to reproduce lattice QCD results. The driving force of the transition, the confinement/deconfinement process, is given a statistical meaning in terms of a reduction of the thermally active partonic degrees of freedom as the critical temperature is approached from above. The fireball evolution is fixed by requiring agreement with hadronic observables at freeze-out [18]. Thermodynamics is calculated along volumes of constant proper time under the assumption of total entropy conservation and using the equation of state (EoS) from lattice QCD as described by the quasi-particle model. In a self-consistent calculational procedure, we determine temperature and volume of the system as a function of proper time.

The main part of the paper is then focused on the kinetic description of charmonium evolution in the fireball.

A transport equation is presented, including dissociation processes in the collision term. In the QGP, Ψ dissociation is provided by the well known Bhanot-Peskin cross section [19, 20]. We also take into account the possibility of Ψ regeneration in the QGP. As recently suggested by several authors [21–24], this process can potentially overwhelm dissociation, leading to Ψ enhancement once the heavy ion collision energy is large enough. The coalescence process of $c\bar{c}$ quark pairs into Ψ is controlled by the cross section obtained from that of dissociation using detailed balance. A simplified, approximate kinetic equation is then obtained. Its solution can be written in closed form, with time dependence entering through the evolution of fireball temperature and volume.

Finally, results for Ψ production at SPS and RHIC are presented and a thorough discussion of theoretical uncertainties concludes the paper.

II. CHARM PRODUCTION OFF NUCLEI: INITIAL CONDITIONS

A. Open charm

The production of charmed quarks is commonly described within perturbative QCD. The perturbative approach is strictly valid only for processes involving large gluon virtualities, usually provided by high-momentum exchange or large masses. In the present case the smallest scale is that of the charm quark mass $m_c \simeq 1.5$ GeV, implying that perturbation theory at lowest order receives important corrections. Moreover, computations are accurate only at large enough transverse momenta p_T , whereas small values of p_T contribute significantly to total yields.

In the following discussion we restrict ourselves to the leading order treatment presented in [25, 26], with suitable adjustments in order to meet phenomenology. We consider the leading processes $q\bar{q} \rightarrow c\bar{c}$ and $gg \rightarrow c\bar{c}$. In terms of their elementary differential cross sections $d\hat{\sigma}_i/d\hat{t}$, the spectrum of c quarks produced in pp collisions at rapidity y_c and transverse momentum p_T is

$$\frac{d\sigma_{pp \rightarrow c}}{dy_c dp_T^2} = K \int dy_{\bar{c}} \sum_{i=u,d,s,g} F_{i/p}(x_1, \mu_c^2) F_{i/p}(x_2, \mu_c^2) \frac{d\hat{\sigma}_i}{d\hat{t}}, \quad (1)$$

where $x_{1,2} = (m_T^c/\sqrt{s}) [\exp(\pm y_c) + \exp(\pm y_{\bar{c}})]$ are the momentum fractions of the partons in the colliding protons and $F_{i/p} = x_i f_{i/p}$. The rapidity variable is defined as usual as $y = 1/2 \log[(E + p_z)/(E - p_z)]$. The factorization scale is taken at $\mu_c = 1.4$ GeV, which is of the order of the c quark mass, and a scaling factor $K = 2$ is used. We employ the GRV94LO [27] parton distributions $f_{i/p}$ and neglect the effect of intrinsic transverse parton momentum. Moreover we set in eq. (1), where appropriate, $m_c = \mu_c$. In this way it is possible to effectively reproduce to good accuracy the next-to-leading order computations for total (y_c - and p_T -integrated) charm produc-

tion as given in [26] and conveniently parametrized in [24] as

$$\sigma_{pp \rightarrow c}^{NLO}(s) = \sigma_c^0 (1 - m_0/\sqrt{s})^{8.185} (\sqrt{s}/m_0)^{1.132}, \quad (2)$$

where $\sigma_c^0 = 3.392 \mu\text{b}$ and $m_0 = 2.984 \text{ GeV}$.

To estimate the spectrum of c quarks in AB collisions, the simplest approach is to scale the pp result with the overlap function

$$T_{AB}(b) = \int d^2r T_A(r) T_B(\tilde{r}) \quad (3)$$

where $T_{A,B}(b) = \int dz \rho_{A,B}(z, b)$ are the usual overlap functions, expressed in terms of longitudinal integrals over the nuclear densities $\rho_{A,B}$, and $\tilde{r} = |\vec{b} - \vec{r}|$, being \vec{r} the transverse coordinate and \vec{b} the impact parameter.

On the other hand, as the collision energy increases, shadowing effects are expected to become important, reducing the total yield [28]. Another correction to be introduced is the broadening effect on the colliding partons' transverse momenta, resulting in a broader p_T spectrum of produced charmed quarks. For simplicity we neglect these effects, thereby obtaining an upper limit for the c quark production cross section. The charmed quark spectrum in AB collisions is then computed as

$$\frac{dN_{AB}^c}{dy_c dp_T^2}(b) = \frac{d\sigma_{pp \rightarrow c}}{dy_c dp_T^2} T_{AB}(b). \quad (4)$$

The total number of charm quarks produced, for example, in a $Au+Au$ collision can be obtained by integrating the spectrum given in the latter equation. The result is shown in Fig. (1). One observes a great difference between the values at SPS and RHIC energies, amounting to nearly two orders of magnitude. Moreover, note that

$$N_{AB}^c(s) = \sigma_{pp \rightarrow c}(s) T_{AB}(b) = N_{pp}^c(s) N_{AB}^{coll}(b), \quad (5)$$

where $N_{pp}^c = \sigma_{pp \rightarrow c}/\sigma_{pp}^{in}$ and $N_{AB}^{coll}(b) = \sigma_{pp}^{in} T_{AB}$, being σ_{pp}^{in} the inelastic pp cross section. Since for large nuclei $N_{AB}^{coll}(b=0) > 1000$, it is clear how many more c quarks are produced in a AB collision with respect to the pp case.

B. Hidden Charm

The description of charmonium production in nuclear collisions is a more complicated task as compared to open $c\bar{c}$ production. At the root of the problem lies the fact that exclusive production of composite particles in hadronic collisions is basically a non-perturbative process. Only at large transverse momenta it is possible to make robust predictions for the spectra. Nevertheless, at least at the phenomenological level, much work has been done in order to understand the physics underlying the results of several experiments. Let us examine pp collisions

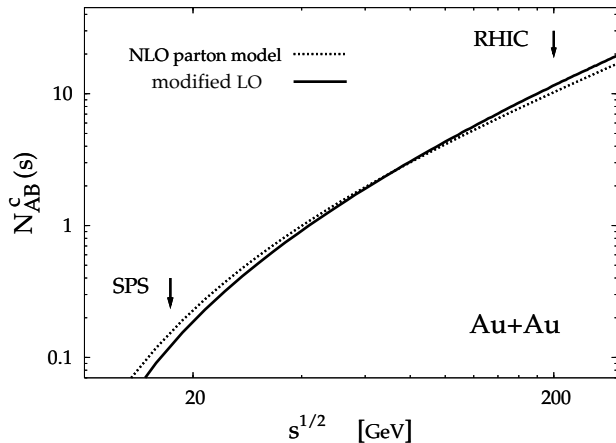


FIG. 1: Number of $c\bar{c}$ pairs produced in a $Au+Au$ collision as function of the center of mass energy, computed by integrating the spectrum given in eq. (4). Curves compare the NLO parton model result (dotted curve) with modified LO calculations with $\mu_c = 1.4 \text{ GeV}$ (solid). From SPS to RHIC energy the number of produced pairs grows by nearly two orders of magnitude

We consider first of all the total production cross section and make use of the parametrization given in [29]. Since it was obtained by fitting low-energy data ($\sqrt{s} < 50 \text{ GeV}$), we modified it to simulate the high energy behavior in terms of NLO effects in the color evaporation model [30]. We parametrize

$$\sigma_{pp \rightarrow J/\psi}(s) = \sigma_{J/\psi}^0 (1 - m_{J/\psi}/\sqrt{s})^9 (1 + 0.6 \sqrt{s}/m_{J/\psi}), \quad (6)$$

with $\sigma_{J/\psi}^0 = 100 \text{ nb}$ and $m_{J/\psi} = 3.1 \text{ GeV}$. The above formula gives essentially identical results as that of [29] in the low energy region and is in line with the recent PHENIX measurement at RHIC [31]. The rapidity modulation can be inferred from the relation $d\sigma/dy \sim x_1 g(x_1) x_2 g(x_2)$ where $g(x) \sim (1-x)^5/x$ is taken to be the gluon distribution in the proton and $x_{1,2} = (m_{\Psi}/\sqrt{s}) \exp(\pm y)$. We can then write the transverse-momentum-integrated Ψ production spectrum in pp collisions as

$$\frac{d\sigma_{pp \rightarrow J/\psi}}{dy} = \sigma_{pp \rightarrow J/\psi}(s) F(s, y), \quad (7)$$

where the y -dependent part is

$$\begin{aligned} F(s, y) &= C(s) (1 - x_1)^5 (1 - x_2)^5 \\ &= C(s) \left[1 - 2(m_{J/\psi}/\sqrt{s}) \cosh y + m_{J/\psi}^2/s \right]^5 \end{aligned} \quad (8)$$

while $C(s)$ is chosen to satisfy the normalization constraint $\int dy F(s, y) = 1$. The transverse momentum dependence will not be needed in the following, except for the value of $\langle p_T^2 \rangle$ which can be taken directly from experiment.

We now consider nuclear effects, starting with the simpler case of proton-nucleus (pA) collisions. It has been shown that the experimental results on J/ψ production can be described using

$$\sigma_{pA \rightarrow J/\psi} = \sigma_{pp \rightarrow J/\psi} \int d^2b T_A(b) S_A^{abs}(b) \quad (9)$$

for the total production cross section. The factor

$$S_A^{abs}(b) = \frac{1 - \exp\left[-\sigma_{J/\psi N}^{abs} T_A(b)\right]}{\sigma_{J/\psi N}^{abs} T_A(b)} \quad (10)$$

is the survival probability for J/ψ to escape the nucleus without being dissociated. It includes the effective absorption cross section $\sigma_{J/\psi N}^{abs}$, a quantity of the order of 3 mb for mid-rapidity J/ψ s as measured at $E_{lab} = 800$ GeV at Fermilab, while it amounts to 4–6 mb for mid-rapidity J/ψ s as measured at $E_{lab} = 200 - 400$ GeV at the SPS. The absorption cross section parametrizes various poorly known effects, with varying importance depending on the collision energy. Among those effects are the presence of color non-singlet degrees of freedom in the dynamics of colliding nucleons, initial state parton energy loss and coherence length and shadowing effects. Moreover, $\sigma_{J/\psi N}^{abs}$ contains information on the nuclear absorption of the excited states ψ' and χ_c which feed into the observed J/ψ yield.

A common property of all of the above effects is the approximate linear dependence on the length of the path which J/ψ traverses in the nuclei. It is therefore justified, to first approximation, to use the same ‘‘optical’’ absorption formula eq. (10), provided a re-scaling and re-interpretation of $\sigma_{J/\psi N}^{abs} \rightarrow \sigma_{J/\psi N}^{NUC}$ and $S_{A,B}^{abs} \rightarrow S_{A,B}^{NUC}$ is done.

When looking at J/ψ production in AB collisions, one can estimate the cross section for a given impact parameter by generalizing eq. (9). The effects of the produced medium are the central topic of this paper and will be thoroughly discussed in the following sections. Neglecting them for the moment, one obtains

$$\frac{dN_{AB}^{J/\psi}}{dy}(b) = \frac{d\sigma_{pp \rightarrow J/\psi}}{dy} T_{AB}(b) S_{AB}^{NUC}(b), \quad (11)$$

where all nuclear effects are included in the suppression function

$$S_{AB}^{NUC}(b) = T_{AB}^{-1}(b) \int d^2r T_A(r) S_A^{NUC}(r) T_B(\tilde{r}) S_B^{NUC}(\tilde{r}) \quad (12)$$

which has the obvious property $S_{AB}^{NUC} < 1$ and $S_{AB}^{NUC} \rightarrow 1$ if $\sigma_{J/\psi N}^{NUC} \rightarrow 0$.

Since nuclear effects depend on energy, we have chosen $\sigma_{J/\psi N}^{NUC}(s_0) = 4.5$ mb at the SPS energy $\sqrt{s_0} = 17.3$ GeV ($E_{lab} = 158$ GeV) in order to be in agreement with the pA measurement, and assumed the relation

$$\sigma_{J/\psi N}^{NUC}(s) = \sigma_{J/\psi N}^{NUC}(s_0) (s/s_0)^\lambda \quad (13)$$

with $\lambda = 0.12$ in order to simulate nuclear effects as predicted in [11].

III. THERMODYNAMICS OF THE PRODUCED MEDIUM

A. Quasi-particle description of the QGP and the Hadronic EoS

Before we address the question of how to describe the medium produced by a nuclear collision, we need to identify its relevant degrees of freedom. On the theoretical side, information about the QCD medium comes from lattice calculations at finite temperature. Simulations of the pressure, entropy and energy density [2] show a drastic increase in the number of degrees of freedom at a critical temperature of about 170 MeV (for two massless flavors [3]) to about 80% of the value of an ideal gas of quarks and gluons.

A perturbative description of the QGP is, however futile, since thermal perturbation theory is in general insufficient for all temperatures of interest. This is evident, for example, from calculations of the free energy of the QGP [32] or the photon self-energy in the thermal medium [33]. Furthermore, close to T_c we expect intrinsically non-perturbative dynamics to enter: the confinement/deconfinement transition and spontaneous chiral symmetry breaking are not accountable for in an expansion in the coupling constant. In view of these facts, we use a more phenomenological approach to QCD thermodynamics which nevertheless goes considerably beyond commonly used ideal gas models. We have shown recently that it is possible to describe the EoS of hot QCD to a very good approximation by the EoS of a gas of quasi-particles with thermally generated masses, incorporating confinement effectively by a temperature-dependent, reduced number of active degrees of freedom. This reduction is caused by the formation of heavy hadrons or glueballs, with large masses compared to T_c , and accounts for the fact that the QGP does not resemble at all an ideal gas of quarks and gluons as the hadronization temperature is approached. Here we give a short summary of the method and refer the reader to [17] for a more detailed discussion.

From asymptotic freedom, we expect that at extremely high temperatures the plasma consists of quasi-free quarks and gluons. Hard thermal loop (HTL) perturbative calculations find, for thermal momenta, spectral functions of the form $\delta(E^2 - k^2 - m^2(T))$ with $m(T) \sim gT$ [34]. As long as the spectral functions of the thermal excitations at lower temperatures resemble qualitatively this asymptotic form, a quasi-particle description is expected to be applicable. QCD dynamics is then incorporated in the thermal masses of the effective quarks and gluons, plus an extra function, required by thermodynamical consistency, which plays the role of the thermal vacuum energy.

The thermal excitations can then be described by a dispersion equation

$$E_i^2(k, T) = \vec{k}^2 + m_i^2(T), \quad (14)$$

where the subscript $i = g, q$ labels gluons and quarks, respectively. The thermal masses $m_i(T)$ are obtained from the self-energy of the corresponding particle, evaluated at thermal momenta $k \sim T$. Eq. (14) is valid as long as this self-energy is only weakly momentum dependent in the relevant kinematic region. In addition, for a quasi-particle to be a meaningful concept, we require its thermal width to be small. The quasi-particle mass, for instance of gluons, is then

$$m_g(T) = T \sqrt{\frac{N_c}{6} + \frac{N_f}{12}} \tilde{g}(T, N_c, N_f) \quad (15)$$

with the effective coupling specified as

$$\tilde{g}(T, N_c, N_f) = \frac{g_0}{\sqrt{11N_c - 2N_f}} \left(\left[1 + \delta \right] - \frac{T_c}{T} \right)^\gamma. \quad (16)$$

N_c and N_f stand for the number of colors and flavors, respectively. The functional dependence of $m_g(T)$ on T is based on the conjecture that the phase transition is second order or weakly first order which suggests an almost power-like behavior $m \sim (T - T_c)^\gamma$ with some pseudo-critical exponent $\gamma > 0$. Setting $g_0 = 9.4$, $\delta = 10^{-6}$ and $\gamma = 0.1$, the effective mass, as given in eq. (15), approaches the HTL result at high temperatures. The thermal quark mass is modeled similarly. Note that in contrast to previous quasi-particle models extrapolated from HTL calculations [35], the thermal masses used here *drop* as T_c is approached from above. Obviously for $T \gg T_c$ the perturbative limit of $m_g(T)$ and $m_q(T)$ is recovered.

The density of the QGP takes the form

$$n(T) = \sum_{q_i=1}^{N_f} \int \frac{d^3k}{(2\pi)^2} f_{q_i}(k, T) + \int \frac{d^3k}{(2\pi)^2} f_g(k, T), \quad (17)$$

where the distribution functions for quarks and gluons are given by

$$f_{q_i,g}(k, T) = \nu_{q,g} C(T) \left\{ \exp \left[\frac{E_{q_i,g}(k, T)}{T} \right] \pm 1 \right\}^{-1}, \quad (18)$$

being $\nu_q = 12$ and $\nu_g = 16$ the number of spin, flavor and color polarizations of quarks ($N_f = 3$) and gluons, while

$$C(T) = C_0 \left[\left(1 + \delta_c \right) - \frac{T_c}{T} \right]^{\gamma_c} \quad (19)$$

is the *confinement factor*. In order to reproduce lattice QCD thermodynamics for two light quarks and one heavy quark, the parameters take the values $C_0 = 1.16$, $\delta_c = 0.02$ and $\gamma_c = 0.29$. Pressure, energy density and entropy density of the QGP follow accordingly.

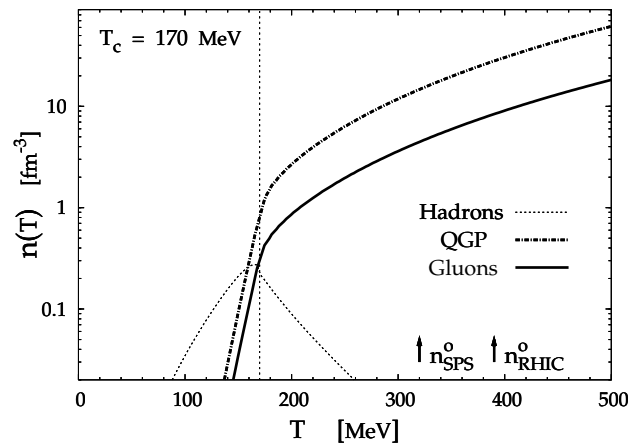


FIG. 2: Particle densities as a function of the temperature T in the hadronic and partonic phases. Here n_{SPS}^0 denotes the initial quasi-particle gluon density at SPS and n_{RHIC}^0 the corresponding value at RHIC. The vertical line indicates the value of the critical temperature $T_c = 170$ MeV.

The driving force of the transition at T_c , the confinement process, is physics that we must include phenomenologically. Below T_c , the relevant degrees of freedom are pions and heavier hadrons. Approaching T_c from below, deconfinement sets in and quark and gluon quasi-particles are liberated. Conversely, when approaching the phase transition from above, the number of thermally active degrees of freedom is reduced due to the onset of confinement. As T comes closer to T_c , an increasing number of quasi-particles gets trapped into hadrons (or glueballs). All confinement does on a large scale is to effectively reduce the number of thermally active degrees of freedom as the temperature is lowered. This effect can be included in the quasi-particle picture by modifying the distribution functions by a temperature-dependent factor $C(T)$ as given in eq. (19). Its explicit form is obtained by calculating the entropy density of the QGP with masses as in eq. (15). Dividing the lattice entropy density by this result yields $C(T)$. Having fixed all parameters by extrapolating available lattice results to realistic zero temperature quark masses, the EoS for two light and a strange quark can be constructed for $T > T_c$.

Below the critical temperature, we employ the EoS of a non-interacting hadronic resonance gas, including all particles up to 1.6 GeV mass. A pion chemical potential is later introduced as a mean to populate the pion phase-space occupation and reproduce the corresponding observed yield. Although this prescription is oversimplified, any improvement has no bearing on the final result of this work. A matching with the high temperature part of the EoS is achieved by smoothly switching off the hadronic degrees of freedom.

It is instructive to plot the total particle density given by eq. (17) as a function of temperature as shown in Fig. 2. The confinement factor $C(T)$ accounts for the

release of the constituents of the hadrons as T grows. Since it does not jump abruptly to one as T_c is reached, some hadronic clusters and hence non-zero hadron densities persist slightly above the critical temperature, as well as quasi-particles persist slightly below T_c . We have indicated the values of particle densities at the beginning and the end of the time evolution of the fireball, as will be discussed in the next section. Comparing the numbers involved, it is obvious that the number density in the QGP is always at least an order of magnitude larger than the hadronic one (note the logarithmic scale). This has a crucial impact on Ψ evolution in the produced medium.

B. Time Evolution of the Fireball

Having characterized the matter which constitutes a strongly interacting system in the thermodynamic limit, we now address the intriguing issue of how this system evolves in time after its production in a heavy-ion collision. Our main assumption is the following: the fireball reaches local thermal (though not necessarily chemical) equilibrium within a time scale of the order of 1 fm/c. We then model the evolution dynamics by calculating the thermodynamic response of the hot and dense matter to the expansion of the total volume. Thermodynamical parameters such as pressure p and energy density ϵ in turn feed back in the expansion dynamics.

We average all quantities over the fireball volume, leaving us with a spatially homogeneous system. The volume itself is taken to be cylindrically symmetric around the beam (z-)axis. In order to account for collective flow, we boost individual volume elements inside the fireball volume with velocities depending on their position. As flow velocities in longitudinal direction turn out to be close to the speed of light, we have to include the effects of time dilatation. On the other hand, we can neglect the additional time dilatation caused by transverse motion, for which the velocity is typically $v_\perp \ll v_z$. The thermodynamically relevant volume is then given by the collection of volume elements corresponding to the same proper time τ . In order to characterize the volume expansion within the given framework, we need first of all the expansion velocity in longitudinal direction as it appears in the center of mass frame. Then we can compute the front position of the expanding cylinder as

$$z(t) = v_z^0 t + \int_{t_0}^t dt' \int_{t_0}^{t'} dt'' a_z(t''), \quad (20)$$

where $a_z(t) = c_z p(t)/\epsilon(t)$ is the longitudinal acceleration and c_z is a parameter. The time t starts running at t_0 such that $z_0 = v_z^0 t_0$ is the initial longitudinal extension, v_z^0 being the initial longitudinal expansion velocity. The longitudinal position $z(t)$ and t itself define a proper time curve $\tau = \sqrt{t^2 - z^2(t)}$. Solving for $\tilde{t} = t(\tau)$ one can construct $\tilde{z}(\tau) = z(\tilde{t})$. Then the position of the fireball front $z(t)$ in the center of mass frame is translated into

the longitudinal extension $L(\tau)$ of the cylinder on the curve of constant proper time τ . One obtains

$$L(\tau) = 2 \int_0^{\tilde{z}(\tau)} ds \sqrt{1 + \frac{s}{\sqrt{s^2 + \tau^2}}}. \quad (21)$$

At the same proper time we define the transverse flow velocity and construct the transverse extension of the cylinder as a disc of radius

$$R(\tau) = R_0 + \int_{\tau_0}^{\tau} d\tau' \int_{\tau_0}^{\tau'} d\tau'' a_\perp(\tau'') \quad (22)$$

where R_0 is the initial overlap root mean square radius of the two colliding nuclei, $a_\perp(\tau) = c_\perp p(\tau)/\epsilon(\tau)$ is the transverse acceleration and c_\perp is a parameter. With values of L and R obtained at a given proper time, the 3-dimensional volume is parametrized as

$$V(\tau) = 2\pi R^2(\tau) L(\tau), \quad (23)$$

where the factor 2 arises from the relation $R_{Box} = \sqrt{2} R_{rms}$ between the radius of a sharp cylinder and its root mean square value.

The model is in principle fully constrained by fitting four parameters: the initial longitudinal velocity v_z^0 , the two constants c_z, c_\perp in a_z, a_\perp and the freeze-out proper time τ_f . These are determined requiring

$$R(\tau_f) = R_f, \quad \frac{dR}{d\tau}(\tau_f) = v_\perp^f, \quad \frac{d\tilde{z}}{dt}(t(\tau_f)) = v_z^f, \quad T(\tau_f) = T_f, \quad (24)$$

where R_f, v_\perp^f, v_z^f and T_f are extracted from an appropriate set of experimental data. In practice this is achieved only at SPS energy for central $Pb + Pb$ collisions, where the freeze-out analysis [36] allows a complete determination. We then assume entropy conservation during the expansion phase, fixing the entropy per baryon s_0 from the number of produced particles per unit rapidity. Calculating the number of participant baryons as

$$N_p(b) = \int d^2r T_A(r) \left\{ 1 - \exp \left[-\sigma_{pp}^{in} T_B(\tilde{r}) \right] \right\} + (A \leftrightarrow B), \quad (25)$$

where $\sigma_{pp}^{in} = 30$ mb at $\sqrt{s} = 17.3$ GeV (SPS) and $\sigma_{pp}^{in} = 42$ mb at $\sqrt{s} = 200$ GeV (RHIC), and scaling the entropy with the calculated number of participants, we find $S_0 = s_0 N_p$, the total entropy. The entropy density at a given proper time is then determined by $s(\tau) = S_0/V(\tau)$. Using the EoS given by the quasi-particle approach, thereby providing constraints from lattice QCD, we find $T(s(\tau))$ and also $p(\tau)$ and $\epsilon(\tau)$. The set of equations (20-23) is then solved iteratively, keeping the entropy constant. Finally we arrive at a thermodynamically self-consistent model for the fireball which is, by construction, able to reproduce the hadronic momentum spectra at freeze-out. This framework was shown to be a key ingredient for a successful description of the low- and intermediate-mass dilepton yields in SPS collisions (see [18] where the model is also described in more detail).

While the fireball evolution is fully constrained by data for central collisions at SPS, an extension towards different impact parameters and higher beam energies is not on the same firm ground. Unfortunately, no detailed freeze-out analysis has been done so far for different centralities, even at SPS. One has to rely on sensible assumptions in order to construct the fireball evolution.

Concerning the impact parameter dependence, from geometric considerations one can compute the overlap area and convert it, for simplicity, to a disc, while maintaining cylindrical symmetry but ignoring all effects of elliptic flow. This approximation should still be valid for not too large impact parameters. Note that the model is not applicable for very peripheral events, since the assumption of thermalization ceases to be valid. We then make the following two assumptions: first, the initial velocity v_z^0 of the fireball front is an important quantity which must change for more peripheral collisions. We consider the empirical fact that in pp collisions leading particles loose on average about one unit of rapidity. This is the limit we expect for very peripheral collisions. In order to account for this effect, we assume that the rapidity loss from incoming nuclei to the bulk of the produced matter scales with the number of binary collisions per participant (~ 2.7 for central AB collisions, 1 for pp) and interpolate linearly the value of v_z^0 between these limits. Second, we assume that the freeze-out temperature T_f remains unchanged for different impact parameters. Since the total entropy scales with the number of participants N_p , all parameters are fixed and the fireball evolution can be generalized to non-central collisions.

The extension of the model to higher beam energies poses a more difficult task. The main reason lies in the transition from a baryon-rich to a baryon-poor scenario. While such an analysis is certainly possible with the amount of data collected by RHIC so far, it is a difficult task and has not yet been carried out. For the time being, we aim at a qualitative description and refrain from giving detailed predictions. Assuming that the entropy per participant scales with the total multiplicity, we can calculate the initial entropy S_0 . In order to account for the decreasing baryon density inside the fireball, we assume a rise in the freeze-out temperature from 100 to 130 MeV when going from SPS to RHIC energy. Similarly, we change the EoS in the hadronic part to incorporate the decreasing pion chemical potential with increasing energy (for a more detailed discussion, see [18]). The thermalization time decreases from 1 fm/c at SPS to 0.6 fm/c at RHIC. From dN/dy particle distributions we extract the rapidity extent of hadron spectra to be of 5.5 units, allowing v_z^f to be extracted. Moreover, experimental results indicate that transverse flow and the geometrical freeze-out radius are virtually unchanged from SPS to RHIC energies [37], so we keep these two parameters unchanged from the SPS case. Finally we adjust v_z^0 consistently with the assumed freeze-out temperature.

The model parameters are eventually determined with the self-consistent procedure described above. Relevant

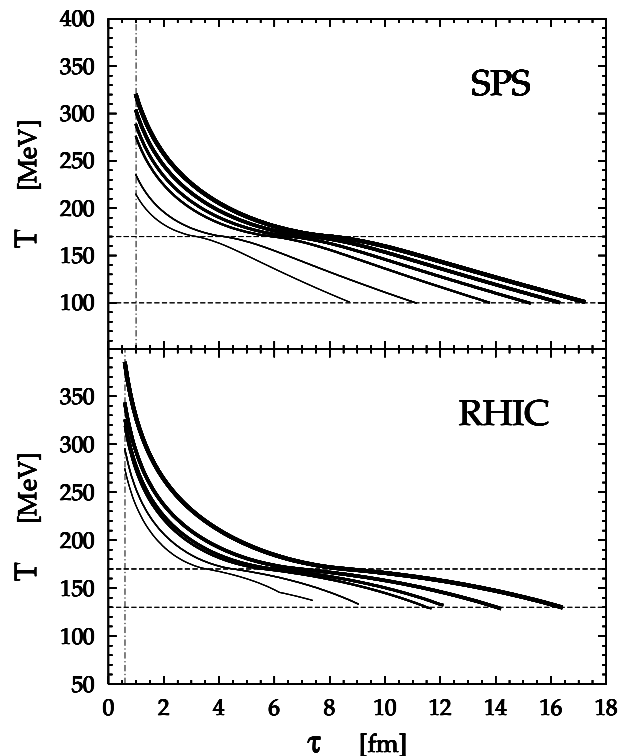


FIG. 3: Temperature T as function of proper time τ for various collisions at SPS and RHIC energies. Curves correspond to impact parameters $b = 0-1$ fm (thicker curves), 2-3, 4-5, 6-7, 8-9 and 10-11 fm (thinner curves).

values of parameters for central collisions at SPS and RHIC are reported in Tab. I. One notices the significant QGP lifetime of about 8 fm, almost half of the total lifetime of the fireball. Temperature T profiles as function of proper time τ for collisions at different impact parameters at SPS and RHIC energies are plotted in Fig. 3. Note the delayed cooling occurring at the transition temperature $T_c = 170$ MeV. This is due to the softening of the

	SPS $Pb+Pb$ $\sqrt{s} = 17.3$ GeV	RHIC $Au+Au$ $\sqrt{s} = 200$ GeV
τ_0	1.0 [fm/c]	0.6 [fm/c]
τ_c	8.0	8.7
τ_f	18	17
T_0	320 [MeV]	390 [MeV]
T_f	100	130
R_0	4.8 [fm]	4.8 [fm]
R_c	5.2	6.0
R_f	9.0	9.0

TABLE I: Key properties of the fireball evolution deduced for central collisions at SPS and RHIC. The numbers given for the radii are root mean square values.

EoS, influencing the volume, and therefore temperature, expansion pattern via the acceleration $a(\tau) \propto p(\tau)/\epsilon(\tau)$ in eqs. (20) and (22). The presence of a longitudinal acceleration term also leads to interesting consequences. The smaller initial rapidity distribution of matter implies a larger initial energy density and hence a higher temperature of the fireball as compared to the Bjorken estimate for these quantities.

Particle densities at the corresponding initial temperatures for central collisions at SPS and RHIC are indicated in Fig. 2 in the previous section.

IV. CHARMONIUM EVOLUTION IN THE EXPANDING MATTER

A. Interaction of Ψ with the produced medium

After having discussed the initial conditions for open and hidden charm production in AB collisions and the physics of the expanding medium, we now come to the central issue of the paper and examine the interaction between charmonium and the produced medium. Because of the relatively small value of the J/ψ formation time

$$\tau_f^\Psi \sim (m_{J/\psi} - m_{\psi'})^{-1} \sim 0.3 \text{ fm}, \quad (26)$$

in the following we will assume that J/ψ s are fully formed hadrons by the time the thermalized medium is produced, and they will subsequently interact with its degrees of freedom. Since the medium itself consists of a QGP for a significantly long time, we begin discussing how J/ψ interacts with quark and gluon quasi-particles. As mentioned in the Introduction, we neglect the possibility of static Debye screening, thereby focusing our analysis on the collisions of Ψ with the QGP degrees of freedom. We argue that a proper treatment of screening and collisions (together, in order to avoid double counting) is a complex dynamical problem involving an unknown time-scale for the modification of the $c\bar{c}$ binding potential. We therefore refrain from speculating on this issue, which deserves a separate study, and simply assume that Ψ s produced by the initial hard processes will propagate and collide with the QGP constituents.

It is clear that collisions of Ψ with either quarks or gluons will lead to dissociation of the bound state. One expects that the two processes illustrated in Fig. (4) contribute to Ψ dissociation in leading order. On the other hand, a quark can interact only via gluon exchange. Within the quasi-particle model, the process labelled (b) in the figure is effectively already included in the definition of the temperature dependent gluon mass. Computing both contributions would lead to an erroneous double counting. In other words, Ψ s only see gluonic quasi-particles in the plasma. As an exception, processes such as $\Psi c \rightarrow gc$ and $\Psi \bar{c} \rightarrow g\bar{c}$ could be important. For example, the first one can proceed by dissociating $\Psi \rightarrow c\bar{c}$ and annihilating the \bar{c} with an incoming c to form a gluon.

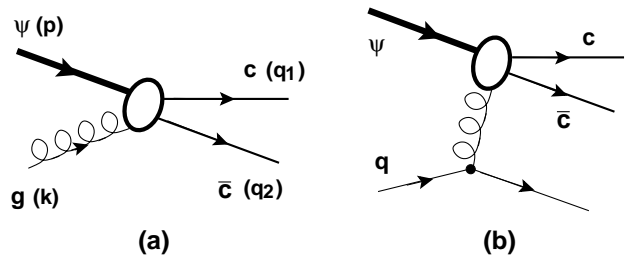


FIG. 4: Diagrams contributing to lowest order to Ψ dissociation. The process involving a gluon quasi-particle (a) exhausts the amplitude since it already takes into account the one involving a quark quasi-particle (b).

Nevertheless such processes can be neglected when compared to gluon dissociation due to the much larger density of the gluons themselves.

We concentrate now on the process (a) in Fig. (4) for the reaction $\Psi(p) + g(k) \rightarrow c(q_1) + \bar{c}(q_2)$, and label momenta as indicated in parentheses. We then come to the problem of computing cross sections involving a relativistic bound state. In the present case one can argue that the $c\bar{c}$ system is, to first approximation, non-relativistic, greatly simplifying the treatment. Moreover, as was done originally by Bhanot and Peskin [19, 20] one can argue that the lowest-lying quarkonium levels can be approximately described using the Coulomb part of the potential. Then, with operator product expansion methods or more recent non-relativistic factorization techniques [38], it is possible to obtain an analytic expression for the cross section. For the case of J/ψ the result is

$$\sigma_{J/\psi g}(\omega) = A_0 \frac{(\omega/\epsilon_{J/\psi} - 1)^{3/2}}{(\omega/\epsilon_{J/\psi})^5}, \quad (27)$$

where $A_0 = (2^{11}\pi/27)(m_c^3 \epsilon_{J/\psi}^0)^{-1/2}$. The cross section is a function of the gluon energy ω in the J/ψ rest frame and involves the threshold energy $\epsilon_{J/\psi}$, related to the binding energy $\epsilon_{J/\psi}^0$ by the condition $(p+k)^2 \geq 4m_c^2$, implying that $\epsilon_{J/\psi} = \epsilon_{J/\psi}^0 + (\epsilon_{J/\psi}^0)^2/(2m_{J/\psi})$. The binding energy is taken to be $\epsilon_{J/\psi}^0 = 800$ MeV and the charm quark mass $m_c = 1.95$ GeV as in [20], to fit the masses of first two charmonium levels ($m_{J/\psi} = 3.1$ GeV and $m_{\psi'} = 3.7$ GeV). In an analogous fashion, it is possible to compute the cross section for ψ' dissociation by gluons. Given the binding energy $\epsilon_{\psi'}^0 = \epsilon_{J/\psi}^0/4$ (for a Coulombic system), and the cross section is

$$\sigma_{\psi' g}(\omega) = 16 A_0 \frac{(\omega/\epsilon_{\psi'} - 1)^{3/2} (\omega/\epsilon_{\psi'} - 3)^2}{(\omega/\epsilon_{\psi'})^7}. \quad (28)$$

Recently also the dissociation cross section for χ_c states was computed [39]. With a mass $m_{\chi_c} = 3.5$ GeV and a

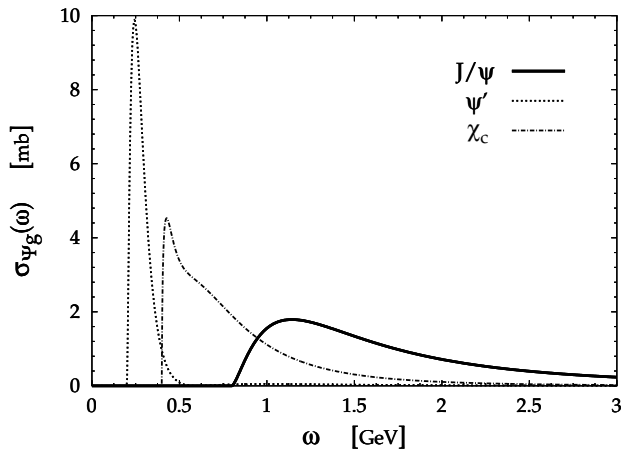


FIG. 5: Dissociation cross sections for the processes $\Psi g \rightarrow c\bar{c}$, where $\Psi = J/\psi, \psi'$ and χ_c , as function of the gluon energy in the rest frame of Ψ .

binding energy $\epsilon_{\chi_c} = 400$ MeV one obtains

$$\sigma_{\chi_c g}(\omega) = 4A_0 \frac{(\omega/\epsilon_{\chi_c} - 1)^{1/2} [9(\omega/\epsilon_{\chi_c})^2 - 20(\omega/\epsilon_{\chi_c}) + 12]}{(\omega/\epsilon_{\chi_c})^7}. \quad (29)$$

The cross sections calculated with eqs. (27), (28) and (29) are not necessarily reliable since the Coulomb potential approximation is used without justification. This problem is serious especially for the ψ' and χ_c states, which have much too large dissociation cross sections. Although the inclusion of higher states is in principle necessary in order to have a reliable description of the dissociation process, since ψ' and χ_c constitute about 40% of the final J/ψ yield, it is not possible at this stage to pursue further this approach. A way out could be to compute these cross section using a realistic potential for the $c\bar{c}$ system, but then questions arise for a rigorous separation of perturbative and non-perturbative contributions and such a study falls beyond the scope of the present treatment. Within the adopted framework we choose to re-scale the ψ' and χ_c cross sections by a multiplicative factor κ such that the obtained J/ψ suppression pattern at SPS energies is in agreement with experiment. The required value is $\kappa = 0.2$ and the resulting cross sections are plotted in Fig. (5). One notices the great difference in magnitude between the J/ψ case as compared to ψ' and χ_c , even after re-scaling. We want to stress the fact that the value $\kappa = 0.2$ is not necessarily large. In fact cross sections are proportional to the square of a matrix element. In the present case, since a gluon is a vector particle, the matrix element consists in a derivative of the Ψ wave function in momentum space. A realistic confining potential would squeeze the spatial wave function more than the Coulomb potential does. In momentum space the wave function would then be more extended and flatter, resulting in a much lower cross section. Within the adopted framework we denote with $\sigma_{\Psi g \rightarrow c\bar{c}}(s)$ the Ψg dis-

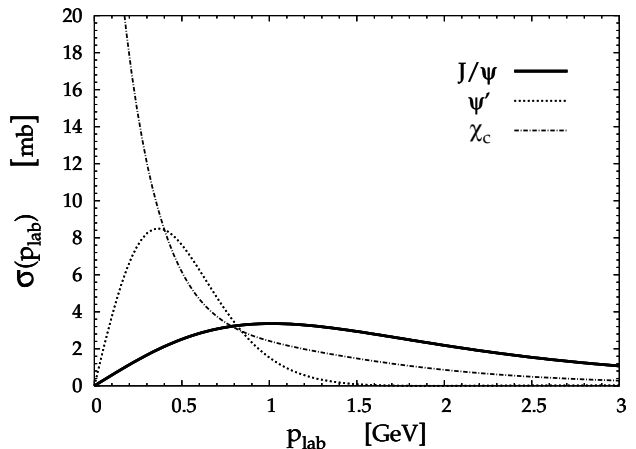


FIG. 6: Formation cross sections for the process $c\bar{c} \rightarrow \Psi g$, where $\Psi = J/\psi, \psi'$ and χ_c , according to eq. (30), as function of the laboratory momentum in the rest frame of the target \bar{c} .

sociation cross section, the dependent variable being the center of mass energy s , related to the gluon energy in the Ψ rest frame as $\omega = k_\mu p^\mu / m_\Psi = (s - p^2 - k^2) / (2m_\Psi)$.

We now consider the possibility of $c\bar{c}$ coalescence in the QGP, a manner for production of Ψ which has been recently considered by several authors. Processes such as $gc \rightarrow \Psi c$ and $g\bar{c} \rightarrow \Psi \bar{c}$ could in principle also contribute, due to the large number of gluons available. On the other hand they require the creation of a $c\bar{c}$ pair from the vacuum and are therefore suppressed. In our formulation we then take into account only the fusion process. We do this by means of a cross section, applying detailed balance to the reaction $\Psi g \leftrightarrow c\bar{c}$, and use the cross section calculated above for Ψ dissociation by gluons. Choosing the zero momentum frame, flux factors are identical for the direct and reverse processes and simple kinematics guarantees that the relation

$$\sigma_{c\bar{c} \rightarrow \Psi g}(s) = \sigma_{\Psi g \rightarrow c\bar{c}}(s) \frac{4}{3} \frac{(s - m_\Psi^2)^2}{s(s - 4m_c^2)} \quad (30)$$

holds. The factor $4/3$ arises from counting the number of degrees of freedom (spin and color factors) in the two different channels. For the Ψg system they are $(1 \times 3) \times (8 \times 2) = 48$, while for the $c\bar{c}$ system $(3 \times 2) \times (3 \times 2) = 36$. Since $s = 2m_c(E_c + m_c)$ for the $c\bar{c}$ system, one can express eq. (30) as function of the c quark momentum p_{lab} in the rest frame of the \bar{c} . The result for $\sigma_{c\bar{c} \rightarrow \Psi g}$ is given in Fig. (6), where the formation cross sections for $J/\psi, \psi'$ and χ_c are shown.

Coming now to the case of hadronic dissociation, we recall that many approaches have been developed in the literature to compute mesonic dissociation cross sections of Ψ . The first calculations were presented in [40]. Subsequently, more sophisticated treatments were developed (See [41] as an example). The resulting thermally averaged cross section amounts to a few mb for the process

$\Psi\rho \rightarrow D\bar{D}$, but computations considered ρ to be a particle with infinite life-time, neglecting its broad spectral function. Accounting for this should considerably reduce the value of the calculated cross section. Significantly smaller values are obtained for $\Psi\pi \rightarrow D\bar{D}$. Despite the efforts applied to perform the mentioned calculations, a realistic time evolution of the fireball was never employed to obtain results comparable with experimental data. We stress that a proper and independent description of the produced medium is crucial if one wants to make use of charmonia as probes of dense matter. In our approach the medium evolution is constrained by the freeze-out analysis, leaving no room for adjustments. According to the calculation of the particle density as function of temperature, plotted in Fig. (2) in the previous section, we see that particle densities in the hadronic phase are almost two orders of magnitude lower than in the QGP phase. Note the logarithmic vertical scale. Unless one employs exceptionally large cross sections, it seems unlikely that hadronic dissociation can be at all relevant. A way out was proposed in [42], where it was argued that the QCD analogue of the Mott transition in an electron plasma may produce an onset behavior in thermally averaged cross section when the Mott temperature $T_{\text{Mott}} \sim T_c$ is reached. However, this framework has not yet been constrained by lattice EoS results. Given the inherent uncertainties and the above remarks on the smallness of particle densities in the hadronic phase, we will not consider the possibility of hadronic dissociation of Ψ .

B. Kinetic Description of Dissociation and Formation

After having discussed and characterized the medium produced in a heavy-ion collision and specified how charmonium interacts by collisions with its constituents, we are ready to address the problem of how produced charmonia evolve and propagate through the medium until their final experimental observation. The natural framework in which to study the time evolution of Ψ is that of kinetic theory. We use a semi-classical treatment, setting up a relativistic kinetic equation for the Ψ phase-space distribution. The general problem of kinetic evolution of bound states in a strongly interacting medium was studied recently [43]. Here we make use of those results, adapting the treatment to our needs. We then assume that the kinetic equation describing the time evolution of the phase-space density f_Ψ of Ψ is

$$p^\mu \partial_\mu f_\Psi(p, x) = C_F^\Psi(p, x) - C_D^\Psi(p, x) f_\Psi(p, x), \quad (31)$$

consisting of the drift term $p^\mu \partial_\mu f_\Psi$ on the l.h.s. and of a collision term on the r.h.s. The collision term is made

of a dissociation (loss) part

$$C_D^\Psi(p, x) = \frac{1}{2} \int d\Phi_3(k, q_1, q_2) (2\pi)^4 \delta^4(p+k-q_1-q_2) \times \overline{W}_{\Psi g \rightarrow c\bar{c}} f_g(k, x) \quad (32)$$

describing Ψ dissociation by quasi-particle gluons, studied in [44, 45] to address the problem of charmonium suppression, and a formation (gain) part

$$C_F^\Psi(p, x) = \frac{1}{2} \int d\Phi_3(k, q_1, q_2) (2\pi)^4 \delta^4(p+k-q_1-q_2) \times \overline{W}_{c\bar{c} \rightarrow \Psi g} f_c(q_1, x) f_{\bar{c}}(q_2, x) \quad (33)$$

describing Ψ formation by $c\bar{c}$ fusion, introduced in a simplified manner in [22]. We stress here that eq. (31) stands actually for 3 equations, for J/ψ , ψ' and χ_c .

In the equations above $f_c, f_{\bar{c}}$ and f_g are the phase-space distributions of the degrees of freedom participating in the collisions. Note that effects of Bose enhancement for gluons and Pauli blocking for c and \bar{c} quarks are negligible. The space-time 4-vector is denoted by x , while kinematics is the same as in the previous section, that is p is the 4-momentum of Ψ , k is that of the gluon, while q_1 and q_2 are those of the c and \bar{c} quarks. The Lorentz invariant 3-body phase-space integration measure is

$$d\Phi_3(k, q_1, q_2) = \frac{d^3k}{(2\pi)^3 2E_k} \frac{d^3q_1}{(2\pi)^3 2E_1} \frac{d^3q_2}{(2\pi)^3 2E_2}. \quad (34)$$

All particles are assumed to be on their mass shells.

The transition probabilities \overline{W} are averaged over the initial color and spin polarizations and summed over the final ones. Without the bar W indicates a transition probability already summed over both initial and final polarizations. Therefore $\overline{W}_{c\bar{c} \rightarrow \Psi g} = N_{c\bar{c}}^{-1} W_{c\bar{c} \rightarrow \Psi g}$ and $\overline{W}_{\Psi g \rightarrow c\bar{c}} = N_{\Psi g}^{-1} W_{\Psi g \rightarrow c\bar{c}}$, with $N_{c\bar{c}} = 36$ and $N_{\Psi g} = 48$. The transition probabilities satisfy detailed balance as

$$W_{c\bar{c} \rightarrow \Psi g} = W_{\Psi g \rightarrow c\bar{c}}. \quad (35)$$

They are related to the cross sections discussed in the previous section, which can be expressed as

$$\sigma_D^\Psi(s) = \frac{1}{4F_{\Psi g}} \int d\Phi_2(q_1, q_2) (2\pi)^4 \delta^4(p+k-q_1-q_2) \overline{W}_{\Psi g \rightarrow c\bar{c}} \quad (36)$$

for dissociation and

$$\sigma_F^\Psi(s) = \frac{1}{4F_{c\bar{c}}} \int d\Phi_2(p, k) (2\pi)^4 \delta^4(p+k-q_1-q_2) \overline{W}_{c\bar{c} \rightarrow \Psi g} \quad (37)$$

for formation. Here the 2-body phase-space integration measure is

$$d\Phi_2(p_a, p_b) = \frac{d^3p_a}{(2\pi)^3 2E_a} \frac{d^3p_b}{(2\pi)^3 2E_b}, \quad (38)$$

while the flux factors are $F_{cd} = \sqrt{(p_c \cdot p_d)^2 - m_c^2 m_d^2}$. In the non-relativistic approximation used in [38], the transition probabilities depend only on the center of mass

energy s . This allows to relate them to the cross sections as

$$\sigma_{ab \rightarrow cd}(s) = \frac{1}{16\pi s} \frac{F_{cd}(s)}{F_{ab}(s)} \overline{W}_{ab \rightarrow cd}. \quad (39)$$

It is then trivial to see that eqs. (35), (36) and (37) are consistent with eq. (30).

Concerning the definitions of the phase-space distribution of gluons, we adopt the expression given in eq. (18) of section III A. The time evolution of the gluon distribution is all contained in the proper time dependence of the temperature. For c quarks, as they are produced in the hard initial collision, we take their spectrum to be given by eq. (4). We assume that they do not interact significantly with the medium, approximately moving on straight lines according to the free streaming equation

$$p^\mu \partial_\mu f_{c,\bar{c}}(q, x) = 0. \quad (40)$$

The initial spatial distribution is assumed to be very narrow. Introducing for convenience the space-time rapidity variable $\eta = 1/2 \log[(t+z)/(t-z)]$, we define the phase-space density of charm quarks as

$$f_c(q, x) = \frac{(2\pi)^3}{\tau m_\perp^c} \frac{dN_{AB}^c}{dy_c d^2\vec{q}_\perp} \delta(y_c - \eta) \rho_\perp(r_\perp(\tau)) \theta(T(\tau) - T_c) \quad (41)$$

and analogously for \bar{c} quarks. The step function θ is introduced to account for the fact that below T_c c and \bar{c} quarks have hadronized into D mesons and are no more available to coalesce into Ψ . For simplicity in later numerical computations, the transverse position density is taken as a box of the same radius of the fireball as

$$\rho_\perp(r_\perp(\tau)) = \frac{1}{\pi R^2(\tau)} \theta(R(\tau) - r_\perp(\tau)), \quad (42)$$

where $\vec{r}_\perp(\tau) = \vec{r}_\perp - (\vec{q}_\perp/m_\perp^c)\tau$. The δ -function, arising from the assumption that c quarks are produced in a very narrow longitudinal region, strongly correlates y_c and η . This is a strong constraint on $c\bar{c}$ coalescence and we will discuss its implications later on.

All the dynamics is now well defined since we have specified the distributions of the medium constituents and those of the bound state constituents, together with the transition probabilities $W_{\Psi g \leftrightarrow c\bar{c}}$. The kinetic equation can be solved exactly in closed form [43]. However, the medium evolution has been constructed by averaging over the whole interaction volume. It is therefore not possible to exploit the full phase-space information contained in eq. (31). We therefore simplify the kinetic equation as follows.

We recall that the Ψ momentum spectrum at a given constant proper time can be computed from the phase-space distribution f_Ψ by means of the Cooper-Frye formula [46]. Integrating out also the transverse momenta, we obtain the Ψ rapidity distribution

$$\frac{dN_\Psi}{dy}(\tau) = \frac{1}{(2\pi)^3} \int d^2p_\perp \int d^2r_\perp d\eta \tau m_\perp^\Psi \cosh(y-\eta) f_\Psi(p, x). \quad (43)$$

If we now re-express the operator $p^\mu \partial_\mu$ appearing in eq. (31) by means of the variables y and η , we obtain

$$p^\mu \partial_\mu = m_\perp \left[\cosh(y-\eta) \frac{\partial}{\partial \tau} + \frac{1}{\tau} \sinh(y-\eta) \frac{\partial}{\partial \eta} \right] + \vec{p}_\perp \cdot \frac{\partial}{\partial \vec{r}_\perp}. \quad (44)$$

It is now simple to see that differentiating with respect to τ the Ψ spectrum given with eq. (43) is equivalent to integrating the l.h.s. of eq. (31) in all phase-space variables except y . More precisely, we obtain

$$\frac{\partial}{\partial \tau} \frac{dN_\Psi}{dy}(\tau) = \frac{1}{(2\pi)^3} \int d^2p_\perp \int d^2r_\perp d\eta \tau p^\mu \partial_\mu f_\Psi(p, x). \quad (45)$$

Integrating the r.h.s. of eq. (31) is a bit more complicated. We first discuss the dissociation term and make use of its definition in eq. (32) and of the definition of dissociation cross section given in eq. (36) to write

$$C_D^\Psi(p, x) = \int \frac{d^3k}{(2\pi)^3 E_k} F_{\Psi g}(s) \sigma_D^\Psi(s) f_g(k, x) f_\Psi(p, x). \quad (46)$$

If we now integrate C_D^Ψ over all phase-space variables except y we obtain

$$\begin{aligned} \int d^2p_\perp d^2r_\perp d\eta \tau C_D^\Psi(p, x) f_\Psi(p, x) &\simeq \\ &\simeq \int \frac{d^3k}{(2\pi)^3} V_{\Psi g} \sigma_D^\Psi(s) f_g(k, T(\tau)) \int d^2r_\perp d\eta \tau E_\Psi f_\Psi(p, x) \\ &\simeq \lambda_D^\Psi(\tau) \frac{dN_\Psi}{dy}(\tau), \end{aligned} \quad (47)$$

where the dissociation rate is defined as

$$\lambda_D^\Psi(\tau) = \int \frac{d^3k}{(2\pi)^3} V_{\Psi g} \sigma_D^\Psi(s) f_g(k, T(\tau)) \Big|_{\substack{y=0 \\ p_\perp = \langle p_\perp \rangle}}. \quad (48)$$

To obtain our result we have made certain approximations. First of all we have suppressed the argument x in f_g since it is redundant, the medium being uniform, and replaced it with the time dependent temperature. The first step to arrive at eq. (47) is obtained approximating the p_\perp dependence of $V_{\Psi g} = F_{\Psi g}(s)/E_\Psi E_k$ and σ_D with its mean value. We neglect for simplicity the dependence of the mean value on centrality and choose $\langle p_\perp \rangle = 2.0$ GeV, whose magnitude is in the range of experimental measurements, for all calculations. Our results are not very sensitive to the precise value of $\langle p_\perp \rangle$, especially after folding them with the fireball time evolution. In the second step we assumed that f_Ψ is peaked around values of y close to η , as for the c quark distribution in eq. (41), and set $y = 0$ which is the relevant value for later comparing our final results with experiment. The dissociation rate, after converting it to a dissociation width by changing dimensions from fm^{-1} to MeV, is plotted in Fig. 7. There the temperature dependence for J/ψ , ψ' and χ_c is shown. One notices that the J/ψ width is smaller than the one of χ_c for temperatures below ~ 300 MeV. J/ψ becomes

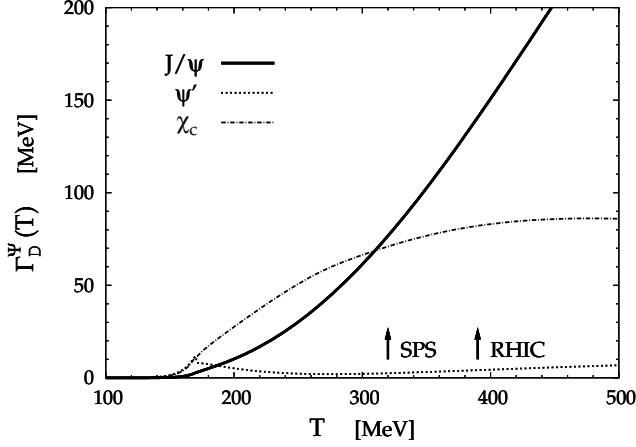


FIG. 7: Dissociation widths of J/ψ , ψ' and χ_c as function of the temperature. Arrows indicate initial temperatures for SPS and RHIC central collisions.

broader at higher temperatures, while the χ_c width stays virtually constant. Notice that the effect on ψ' is negligible. The different behaviors are related to the different forms and thresholds of the dissociation cross sections, as illustrated in Fig. 5.

Considering now the formation term on the r.h.s. of eq. (31), we integrate C_F^Ψ in the same way as for C_D^Ψ over the phase-space variables and define the formation rate

$$\lambda_F^\Psi(\tau) = \frac{1}{(2\pi)^3} \int d^2 p_\perp \int d^2 r_\perp d\eta \tau C_F^\Psi(p, x) \Big|_{y=0}. \quad (49)$$

Its detailed evaluation proceeds without approximations but goes through several steps. We leave all details in the Appendix and here report the final result which is

$$\lambda_F^\Psi(\tau) = \frac{1}{\tau} \int d^2 p_\perp d^2 q_\perp d^2 q_\perp^2 K \sigma_F^\Psi(s) S_c(\bar{y}_c, q_\perp) S_c(\bar{y}_c, q_\perp^2) \quad (50)$$

where K is a dimensionless quantity given in eq. (A.6), while $S_c(y, q_\perp)$ is the c quark spectrum as given in eq. (4). The resulting formation rate $\lambda_F^0 = \lambda_F^\Psi(\tau_0)$ is plotted for J/ψ , ψ' and χ_c in Fig. 8 at the initial evolution time, as function of the collision energy. The values increase by more than three orders of magnitude from SPS to RHIC central collisions, thereby suggesting that the mechanism of Ψ formation by $c\bar{c}$ coalescence might be important at high energies.

With all the simplifications mentioned before, we have managed to reduce eq. (31) to a simple first order differential equation for the rapidity distribution of Ψ as function of proper time. In fact, putting together eqs. (45), (47) and (49) we obtain that

$$\frac{\partial}{\partial \tau} \frac{dN_\Psi}{dy}(\tau) = \lambda_F^\Psi(y, \tau) - \lambda_D^\Psi(y, \tau) \frac{dN_\Psi}{dy}(\tau), \quad (51)$$

whose solution, valid at $y = 0$, is obtained with few elementary steps and provides the final Ψ rapidity distribu-

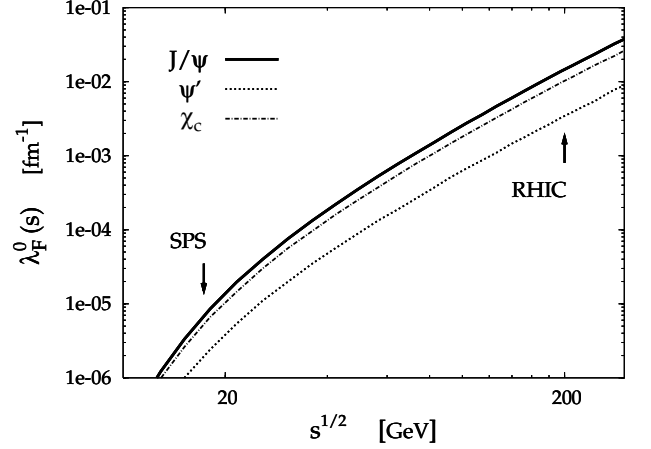


FIG. 8: Formation rates of J/ψ , ψ' and χ_c computed at the initial evolution time as function of the collision energy. The values increase by more than three orders of magnitude from SPS to RHIC central collisions.

tion at $y = 0$ as

$$\frac{dN_\Psi^f}{dy} = \left\{ \frac{dN_\Psi^0}{dy} \exp \left[- \int_{\tau_0}^{\tau_f} d\tau' \lambda_D^\Psi(y, \tau') \right] + \int_{\tau_0}^{\tau_f} d\tau' \lambda_F^\Psi(y, \tau') \exp \left[- \int_{\tau'}^{\tau_f} d\tau'' \lambda_D^\Psi(y, \tau'') \right] \right\}. \quad (52)$$

Again, the solution found holds for the different charmonia J/ψ , ψ' and χ_c . The initial condition dN_Ψ^0/dy is given by eq. (11) and the rates λ_D^Ψ and λ_F^Ψ are given respectively by eqs. (48) and (50). Note that they are implicitly dependent on impact parameter and collision energy. The structure of this solution is self-evident. The first term describes the dissociation of Ψ s initially produced in the hard collision, with the usual exponential suppression acting at all times from τ_0 to τ_f , while the second term describes formation of Ψ s from $c\bar{c}$ in the QGP, from the initial time τ_0 up to an intermediate value τ' and their subsequent suppression from τ' to τ_f , integrated over all values of τ' . This last term may become important as soon as the number of charmed quarks is large enough. This is expected to be the case in AB reactions as the collision energy increases, since the c quark spectrum is proportional to the mean number of nucleon-nucleon collision $N_{coll} > 1000$ for large nuclei, and because the magnitude of the spectrum grows by nearly two orders of magnitude from, say, SPS to RHIC energy, as shown in Fig. 1.

As a final remark we stress that leaving the y -integration open is important since we are interested in computing the value of the final Ψ rapidity distribution at mid-rapidity, and not the whole yield, for which experimental results are available and with which we want to confront our model.

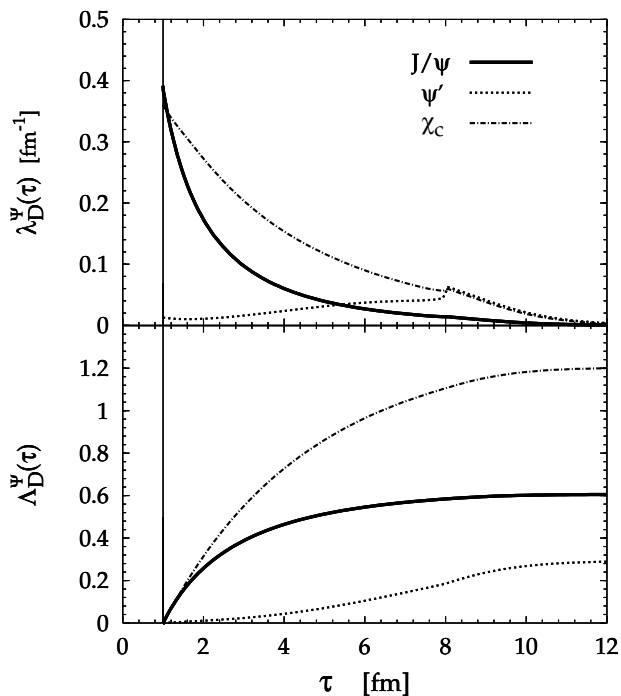


FIG. 9: Top: time evolution of dissociation rates $\lambda_D^\Psi(\tau)$ for J/ψ , ψ' and χ_c , defined in eq. (48), computed for central collisions at SPS energy. Bottom: same as above for the integrated dissociation rates $\Lambda_D^\Psi(\tau)$.

C. Results

Using the elements of the calculation as discussed in the previous sections, we can now compute the time dependence of dissociation and formation rates. The dissociation rate depends on the fireball temperature which, in turn, depends on time. How T depends in detail on τ , was evaluated for different impact parameters and collision energies in section III B. For central collisions at SPS energies (for RHIC conditions the result is qualitatively similar), the dissociation rates λ_D^Ψ , defined in eq. (48) are plotted against τ in Fig. 9 (top). For J/ψ it drops fast, initially approximately as $1/\tau$, for χ_c the rate drops more slowly, while for ψ' it is maximum at hadronization. The integrated rates, denoted by Λ_D^Ψ , constitute the exponents of the suppression factors in eq. (52). They are also plotted in Fig. 9 (bottom). All curves level off after hadronization in a similar way and the final value for χ_c dominates the others.

Analogously, we computed the formation rates λ_F^Ψ , defined in eq. (50), which depend on time via the factor $1/\tau$ and a factor $1/R^2(\tau)$, contained in the quantity K given with eq. (A.6). It turns out that the coalescence mechanism is ineffective at SPS energies, therefore we plot the formation rate against time, for central RHIC collisions, in Fig. 10 (top). For all charmonia the formation rates drop faster with increasing τ than the dissociation rates. They are negligible well before hadronization occurs. The

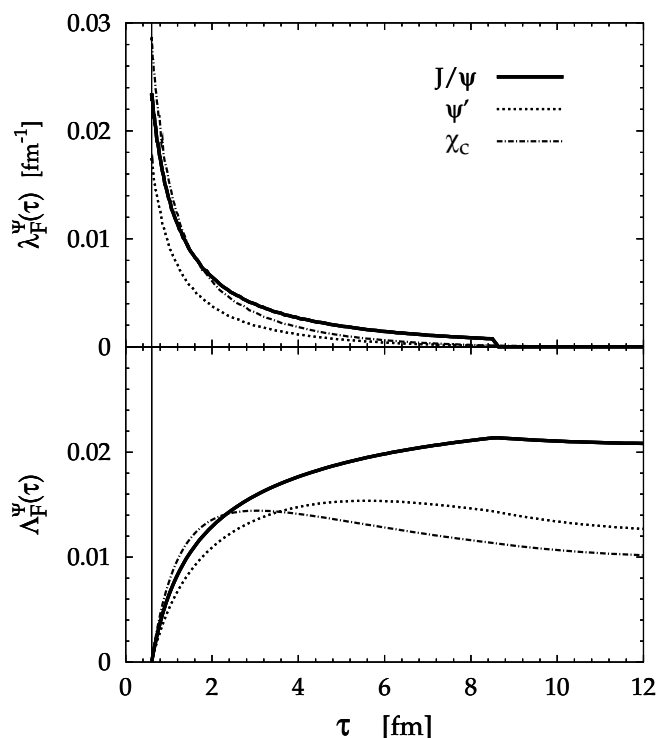


FIG. 10: Top: time evolution of formation rates $\lambda_F^\Psi(\tau)$ for J/ψ , ψ' and χ_c , defined in eq. (50), computed for central collisions at RHIC energy. Bottom: same as above for the integrated formation rates $\Lambda_F^\Psi(\tau)$ weighted by the suppression factor as in the r.h.s. of eq. (52).

integrated formation rate is folded with the exponential suppression factor and computed as in the second term on the r.h.s. of eq. (52), denoting it by Λ_F^Ψ . The result is plotted also in Fig. 10 (bottom). Obviously all curves level off before hadronization, showing a dominance of $c\bar{c}$ coalescence into J/ψ rather than in ψ' or χ_c . Noteworthy is the tendency of the Λ_F^Ψ to decrease once again at later times, when the λ_F^Ψ are by then small and dissociation tends to take over. This behavior is more pronounced for χ_c , for which dissociation is still strong in the vicinity of hadronization.

Dissociation and formation rates are then combined together according to eq. (52) to give the observed Ψ rapidity distribution. As the fireball evolution is constructed for different impact parameters and collision energies, we compute the corresponding rapidity distribution at $y = 0$.

Since we are interested for the final J/ψ yield, we need to take into account decays into the charmonium ground state of ψ' and χ_c . Experimentally it has been observed that measured J/ψ s come in a fraction of 60% from direct production, while a fraction of 10% comes from ψ' decays and a fraction of 30% is from χ_c . Denoting these fractions as $W_{J/\psi} = 0.6$, $w_{\psi'} = 0.1$ and $w_{\chi_c} = 0.3$, we

can write the final J/ψ rapidity distribution as

$$\frac{dN_{J/\psi}^{fin}}{dy} = \sum_{\Psi} W_{\Psi} \frac{dN_{\Psi}^f}{dy}, \quad (53)$$

where the sum extends over $\Psi = J/\psi, \psi', \chi_c$. Approximating the weighted exponential for suppression of the initially produced J/ψ s, implicit in eq. (53) and appearing in eq. (52), as

$$\begin{aligned} \sum_{\Psi} W_{\Psi} \frac{dN_{\Psi}^0}{dy} \exp \left[- \int_{\tau_0}^{\tau_f} d\tau' \lambda_D^{\Psi}(y, \tau') \right] \\ \simeq \frac{dN_{J/\psi}^0}{dy} \sum_{\Psi} W_{\Psi} \exp \left[- \int_{\tau_0}^{\tau_f} d\tau' \lambda_D^{\Psi}(y, \tau') \right], \end{aligned} \quad (54)$$

which is correct to leading order in the expansion of the exponential, we obtain the final form of the J/ψ rapidity distribution which can be compared with experimental data. The required expression is

$$\begin{aligned} \frac{dN_{J/\psi}^{fin}}{dy} = & \left\{ \frac{dN_{J/\psi}^0}{dy} \sum_{\Psi} W_{\Psi} \exp \left[- \int_{\tau_0}^{\tau_f} d\tau' \lambda_D^{\Psi}(y, \tau') \right] \right. \\ & \left. + \sum_{\Psi} W_{\Psi} \int_{\tau_0}^{\tau_f} d\tau' \lambda_F^{\Psi}(y, \tau') \exp \left[- \int_{\tau'}^{\tau_f} d\tau'' \lambda_D^{\Psi}(y, \tau'') \right] \right\}. \end{aligned} \quad (55)$$

We now look at the case of $Pb+Pb$ collision at $\sqrt{s} = 17.4$ GeV and compute the J/ψ spectrum as function of the impact parameter b . Then we construct the $J/\psi/DY$ ratio

$$\begin{aligned} R_{J/\psi/DY}(b) &= B_{\mu^+\mu^-} \frac{dN_{J/\psi}(b)/dy}{dN_{DY}(b)/dy} \\ &= B_{\mu^+\mu^-} \frac{dN_{J/\psi}(b)/dy}{dN_{DY}^{pp}/dy N_{coll}(b)} = N_0 \frac{dN_{J/\psi}(b)/dy}{dN_{\Psi}^{pp}/dy N_{coll}(b)}, \end{aligned} \quad (56)$$

where we assume that the Drell-Yan spectrum in $Pb+Pb$ collisions scales with the number of collisions N_{coll} . The coefficient $B_{\mu^+\mu^-}$ is the branching of J/ψ into $\mu^+\mu^-$ pairs. The overall normalization is fixed at $N_0 = 53.5$ to match, at large values of b , the experimental value in pp collisions. The $J/\psi/DY$ ratio is then plotted in Fig. 11 (solid line) as function of the mean transverse energy

$$E_T(b) = \epsilon_T N_p(b). \quad (57)$$

The quantity $\epsilon_T = 0.274$ is the amount of produced transverse energy per participant. As reference, we also plot the curve obtained by considering only nuclear effects (dotted line) and neglecting the contribution of the produced medium. The agreement with data is quite remarkable, in particular the slope of the curve, considering that fireball parameters have not at all been tuned to this particular observable. The result as such deserves some detailed comments. First of all, for simplicity we do not perform the usual convolution with the $E_T - b$ correlation function [13], therefore it is obvious that the curves end

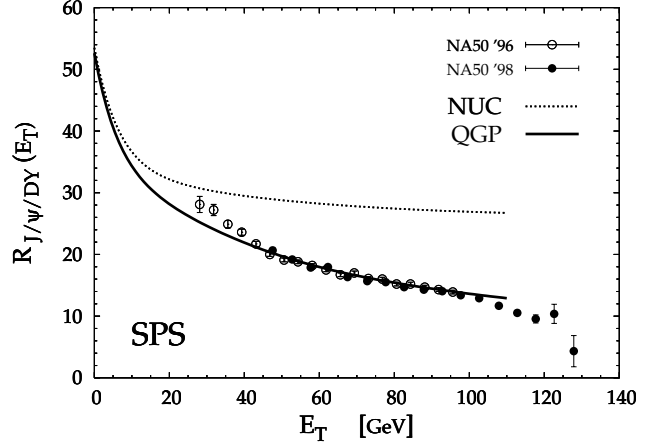


FIG. 11: Result at SPS energy for the $J/\psi/DY$ ratio as function of the transverse energy. The dotted curve, labelled “*NUC*”, includes only nuclear effects, while the solid line, labelled “*QGP*”, is the complete result including dissociation by collisions with gluonic quasi-particles.

at $E_T \simeq 110$ GeV, which corresponds to the mean transverse energy at $b = 0$. To go beyond this point and be in agreement with the data it is necessary to include effects of fluctuations, which can be treated in a straightforward manner [47]. Second, we find that the formation mechanism of J/ψ by $c\bar{c}$ coalescence is totally negligible at this energy, while suppression is caused exclusively by collisions with gluonic quasi-particles. Third, hadronic dissociation of J/ψ seems to be ruled out, not because cross sections are small, rather because the hadronic number density is more than an order of magnitude lower than the partonic one, and only a fraction of a fm^{-3} already at hadronization. All this was clearly shown in Fig. 2. This last statement relies on the fact that the time evolution of the fireball is not constructed *ad hoc* in order to obtain the desired result, but a priori and with independent experimental information (hadronic and low-mass dilepton spectra). Last, the low E_T region is over-estimated in our result. This is mainly due to the too simple scaling with the number of participants, neglecting the fact that for central collisions the amount of produced transverse energy receives a contribution from the mean number of collisions. In any case, the fireball description is not expected to be valid at large impact parameters.

As we now increase the collision energy, staying at impact parameter $b = 0$, we observe an interesting feature. Since the amount of charmed quarks grows substantially with increasing energy, as was indicated in Fig. 1, we expect that the formation of J/ψ s via $c\bar{c}$ coalescence can become important and at least comparable to the primordial one. To study this we construct the suppression function

$$S_{J/\psi}(s) = \frac{dN_{J/\psi}(s, b=0)/dy}{dN_{J/\psi}^{pp}(s)/dy N_{coll}(b=0)} \quad (58)$$

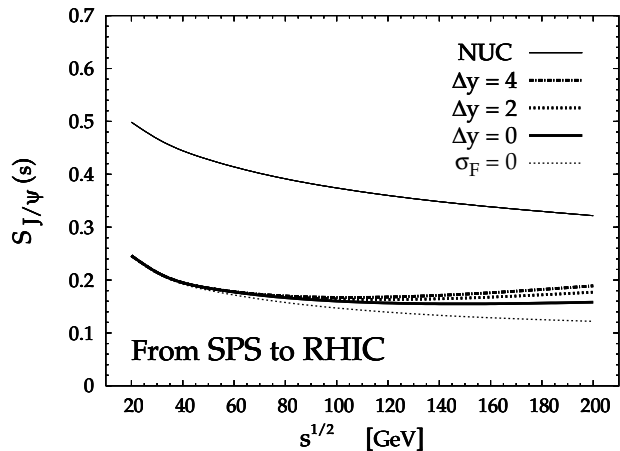


FIG. 12: Suppression factor $S_{J/\psi}$ as function of the collision energy. The thin solid line labelled “ NUC ” is computed with nuclear effects alone. The thin dotted line labelled “ $\sigma_F = 0$ ” is the result with only J/ψ dissociation. The thick solid line labelled “ $\Delta y = 0$ ” is the full calculation. The thick dotted and dot-dashed lines, labelled “ $\Delta y = 2$ ” and “ $\Delta y = 4$ ” respectively, are obtained by relaxing the assumption of complete $y_c - \eta$ correlation, as explained in the text.

and look at its dependence on s . Note that in absence of nuclear or medium effects one should have $S_{J/\psi} \equiv 1$. Indications of the onset of the formation mechanism clearly appear from our calculations, which we plot in Fig. 12. The thin solid line labelled “ NUC ” represents the suppression function when only nuclear effects are included. According to eq. (13) the effective absorption cross section is $\sigma_{\Psi}^{NUC}(\sqrt{s} = 200 \text{ GeV}) = 8.2 \text{ mb}$. The thin dotted line labelled “ $\sigma_F = 0$ ” is the result with only Ψ dissociation, without the formation mechanism. The thick solid line labelled “ $\Delta y = 0$ ” is the full calculation. One clearly observes, especially at the full RHIC energy, a substantial contribution of about 30% of the total from the formation mechanism. The thick dotted and dashed lines, labelled “ $\Delta y = 2$ ” and “ $\Delta y = 4$ ” are obtained by relaxing the assumption of complete $y_c - \eta$ correlation realized by the δ -function in eq. (41). This is done approximately by smearing the latter with a Gaussian of width Δy . The values chosen are $\Delta y = 0$, the baseline value, and $\Delta y = 2, 4$. More details are given at the end of the Appendix. Smearing the $y_c - \eta$ correlation allows the formation mechanism to become more efficient, leading to a J/ψ yield of comparable magnitude with the primordial one. The net effect is a slowly rising function of \sqrt{s} , but in any case we still have suppression, even at RHIC energy.

We now proceed to examine central collisions at RHIC energy. In order to compare with preliminary data from the PHENIX experiment [31], obtained at mid-rapidity from Ψ decays into e^+e^- pairs, we construct the quantity

$$N_{J/\psi}^*(b) = B_{e^+e^-} \frac{dN_{J/\psi}(b)/dy}{N_{coll}(b)} \quad (59)$$

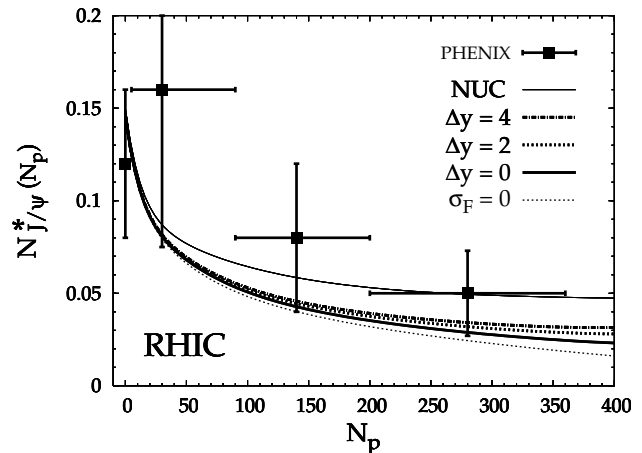


FIG. 13: Result at RHIC energy for the J/ψ yield, scaled by the number of binary collisions, as function of the number of participants. Different line types for the curves and their labels are described in Fig. 12. Filled squares are preliminary PHENIX data.

and plot it in Fig. 13 as function of the number of participants. The quantity $B_{e^+e^-}$ is the branching of J/ψ into e^+e^- pairs, while the overall normalization is fixed at $N_{J/\psi}^*(N_p = 0) = 0.15$. We label all curves consistently with Fig. 12. Although a comparison with the data is, at present, premature, we see that our results lie within experimental errors. Again, the contribution from $c\bar{c}$ coalescence into J/ψ is significant, although not dramatic. All the obtained curves are monotonically decreasing and we do not find any inversion of this tendency at any large value of N_p . In other words, we do not find a net enhancement of J/ψ , but this result needs to be confirmed by more accurate calculations. The reasons are twofold: first, although we have a rough picture of what medium to expect at RHIC, the corresponding fireball is presently not yet determined at the same level of quality as with existing SPS data. Second, shadowing effects for J/ψ production have been taken into account only very crudely. For open charm production also recent calculations [28] show a non negligible amount of shadowing. Indeed, the expectation at RHIC energy is a reduction of dN_{AB}^c/dy by about 30% at mid-rapidity. The resulting reduction factor of 0.7 enters squared in the formation rate given on the right of eq. (50), therefore reducing by about half the enhancement effect.

D. Remarks on the QGP at SPS

Consider once again the solution of the kinetic equation given as eq. (52) and neglect the formation term. Taking the time evolution of the medium density in the simple form $n(\tau) = n_0 \tau_0/\tau$ and assuming that the average dissociation cross section is time independent (denoted by

σ_D), we obtain the simple analytical solution

$$\frac{dN_{J/\psi}^f}{dy} = \frac{dN_{J/\psi}^0}{dy} \exp \left[-\sigma_D n_0 \tau_0 \log(n_0/n_f) \right], \quad (60)$$

where $n_f = n(\tau_f)$. We examine the exponential suppression factor for parameter values corresponding to the situation in central collisions at the SPS. We assume that the produced QGP is thermalized so that the gluon density is given, in the ideal gas limit, by

$$n(T) = \frac{g\zeta(3)}{\pi^2} T^3. \quad (61)$$

The final density is fixed by eq. (61) at the critical temperature $T_c = 170$ MeV, yielding $n_f = 1.25 \text{ fm}^{-3}$. Taking $\sigma_D = 1$ mb and $\tau_0 = 1$ fm, consistently with what has been computed earlier in the previous sections, one needs $n_0 = 5 \text{ fm}^{-3}$ in order to have a suppression factor of about 0.5, which is precisely the amount of anomalous suppression required by the NA50 data at large E_T . Note that the initial density required in this scenario corresponds to $T_0 = 270$ MeV.

We now compare the above estimate with the results given by a popular model [48], describing J/ψ suppression by means of collisions with comovers, usually considered to belong to the class of “hadronic models”. Its essential element is the suppression function

$$S(\vec{b}, \vec{r}) = \exp \left[-\sigma_{co} N_y^{co}(\vec{b}, \vec{r}) \log(N_y^{co}(\vec{b}, \vec{r})/N_f) \right], \quad (62)$$

where $\sigma_{co} = 1$ mb represents the interaction with comovers, $N_y^{co}(\vec{b}, \vec{s})$ is the 2-dimensional rapidity density of hadrons as function of the transverse coordinate \vec{r} for a given impact parameter \vec{b} , computed in the Dual Parton Model [49], and $N_f = 1.15 \text{ fm}^{-2}$. Averaging S by means of the “production probability” $T_A T_B$ and neglecting nuclear effects, we obtain

$$\langle S \rangle(\vec{b}) \approx \exp \left[-\sigma_{co} N_y(b) \log(N_y(b)/N_f) \right], \quad (63)$$

where the average rapidity density of comovers is computed as

$$N_y(b) = \frac{\int d^2r T_A(r) T_B(\vec{r}) N_y^{co}(\vec{b}, \vec{r})}{\int d^2r T_A(r) T_B(\vec{r})}. \quad (64)$$

If we now identify

$$\sigma_D = \sigma_{co}, \quad n_0 \tau_0 = N_y(b=0) \quad \text{and} \quad n_f \tau_0 = N_f, \quad (65)$$

we immediately recover the suppression factor in eq. (60). Computing numerically eq. (64) at $b = 0$, we obtain $N_y = 6 \text{ fm}^{-2}$, which should be compared with the product $n_0 \tau_0 = 5 \text{ fm}^{-2}$. The numerical agreement is quite striking. To show that this is not a mere coincidence, we can compare the final values for the densities. Numerically this means to confront $N_f = 1.15 \text{ fm}^{-2}$ with

$n_f \tau_0 = 1.25 \text{ fm}^{-2}$ determined above: again, a remarkable agreement. It is clear that the initial density of “hadrons” as computed with the Dual Parton Model is far too high for the medium to be “hadronic”, and the particle density N_f is not to be understood as the freeze-out value but rather to be taken at hadronization. It is therefore suggestive to interpret the comover model as actually describing anomalous J/ψ suppression by the QGP.

V. CONCLUSIONS

We have calculated J/ψ production from an expanding fireball created in relativistic heavy-ion collisions over a wide range of centralities and beam energies, from SPS at $\sqrt{s} = 17.3$ GeV ($E_{lab} = 158$ GeV) to RHIC at $\sqrt{s} = 200$ GeV. In this summary we review our basic assumptions put them into perspective.

The produced medium was described assuming QGP formation and thermalization. A phenomenological quasi-particle model for quarks and gluons, in accordance with lattice QCD thermodynamics, was applied to model the partonic phase. This provided a realistic EoS which we then used to drive the expansion dynamics of the medium by means of a fireball model, characterized by time dependent temperature and volume. This construction had already been proven successful in describing low mass dilepton spectra at SPS. We want to stress again that the setup of this fireball (initial and freeze-out temperature, density etc.) had been fixed by independent observables and ensures consistency with a multitude of hadronic measurements. In contrast to previous approaches, we have therefore largely eliminated the medium evolution as an adjustable parameter in the J/ψ description. Nevertheless, this framework is still simplified and is probably insufficient to account for phase-space correlations of the medium, which have been averaged out. In a future attempt to study rapidity and p_\perp -dependent properties of J/ψ , this is a problem to be taken into account.

We then set up a kinetic equation with a collision term incorporating both gain and loss terms. These stand for Ψ formation due to coalescence of $c\bar{c}$ quark pairs and Ψ dissociation due to collisions with gluon quasi-particles, respectively. The elementary process $\Psi g \rightarrow c\bar{c}$ was modeled by a simplified dissociation cross section, approximating Ψ as a Coulomb bound state. The corresponding back reaction $c\bar{c} \rightarrow \Psi g$ could then be obtained by detailed balance. Here a few important remarks are necessary. First of all, a crucial ingredient for the construction of the solution of the kinetic equation is a reliable initial condition. In the present work we have simplified this aspect in order to focus on the QGP effects, but it is possible to improve on this point, especially in what concerns the description of nuclear effects, both for open and for hidden charm. New data collected at RHIC in recent deuteron+Au collisions will certainly help constraining

the model dependence of such calculations. Second, the description of medium effects on Ψ was developed neglecting screening of the $c\bar{c}$ potential. This is an assumption which should be checked by a comprehensive study of the Ψ self energy in a QGP, including, at the same time, screening and collision processes. Third, the use of the Coulomb part of the potential to describe $c\bar{c}$ bound states is only a rough approximation. In fact, cross sections involving ψ' and χ_c had to be rescaled in order to achieve agreement with the data. A proper description of bound states with a realistic potential, including a confining and possibly screened part, is then necessary. Despite such simplifications, the description as a whole seems to be coherent and provides a framework for future developments.

With proper averaging of the kinetic equation over the spatial extent of the fireball, we then found a simple solution, which allowed direct comparison with experiment. At SPS energy we were able to describe the suppression effect in the data, without the need to invoke hadronic comovers. These results support the hypothesis that the QGP is actually produced, at a transient stage, in $Pb+Pb$ collisions at $\sqrt{s} = 17.3$ GeV. It is important to note that, within our outlined approach, a purely hadronic frame-

work would not be successful in describing existing data. Moreover, since the hadronic phase exists only at moderately low particle densities, it has no bearing on Ψ evolution. We also considered extrapolations up to RHIC energies where, despite the more extreme conditions as compared to SPS, a sizable fraction of primordial J/ψ s still survives. Although a clear trend towards more copious J/ψ production in by $c\bar{c}$ coalescence was found, no net J/ψ enhancement was present in the end. This result needs to be confirmed by a dedicated study of space-time and momentum $\eta - y_c$ rapidity correlations for charm quarks, since they have a non-negligible effect on the final results.

Acknowledgements

We are grateful to Peter Braun-Munzinger, Elena Ferreira, Pol-Bernard Gossiaux, Jörg Hüfner and Helmut Satz for stimulating discussions and in particular to David Blaschke for numerous exchanges of opinions during the preparation of this paper. This work was supported in part by BMBF and GSI.

APPENDIX: EVALUATION OF THE COALESCENCE RATE

We evaluate here the coalescence rate. From the definition of the formation term in eq. (33), substituting in it eqs. (34), (39) and (41) we obtain

$$C_F(p, x) = \frac{2\pi^2}{\tau^2} \int \frac{d^3k}{E_k} \frac{d^3q_1}{E_1} \frac{d^3q_2}{E_2} \delta^4(p + k - q_1 - q_2) S_c(y_1, q_\perp^1) S_c(y_2, q_\perp^2) \delta(y_1 - \eta) \delta(y_2 - \eta) \quad (\text{A.1})$$

$$\times \frac{s F_{c\bar{c}}(s)}{m_\perp^1 m_\perp^2 F_{\Psi g}(s)} \sigma_F(s) \frac{1}{[\pi R^2(\tau)]^2} \theta(R(\tau) - |\vec{r}_\perp - (\vec{q}_\perp^1/m_\perp^1) \tau|) \theta(R(\tau) - |\vec{r}_\perp - (\vec{q}_\perp^2/m_\perp^2) \tau|).$$

Integrating over all phase space variables, except for y , we define the formation rate as

$$\lambda_F(\tau) = \frac{1}{(2\pi)^3} \int d^2p_\perp \int d^2r_\perp d\eta \tau C_F(p, x) \Big|_{y=0}$$

$$= \frac{1}{4\pi\tau} \int d^2k_\perp d^2q_\perp^1 d^2q_\perp^2 \int dy_k dy_1 dy_2 \delta(E_\Psi + E_k - E_1 - E_2) \delta(p_z + k_z - q_z^1 - q_z^2) \delta(y_1 - y_2)$$

$$\times \frac{s(s - 4m_c^2)}{m_\perp^1 m_\perp^2 (s - m_\Psi^2)} \sigma_F(s) S_c(y_1, q_\perp^1) S_c(y_2, q_\perp^2)$$

$$\times \int d^2r_\perp \frac{1}{[\pi R^2(\tau)]^2} \theta\left(R(\tau) - |\vec{r}_\perp - \vec{\xi}/2|\right) \theta\left(R(\tau) - |\vec{r}_\perp + \vec{\xi}/2|\right), \quad (\text{A.2})$$

where $\vec{k}_\perp = \vec{q}_\perp^1 + \vec{q}_\perp^2 - \vec{p}_\perp$ and $\vec{\xi} = (\vec{q}_\perp^1/m_\perp^1 - \vec{q}_\perp^2/m_\perp^2) \tau$. The integral over rapidities can be manipulated to give

$$\int dy_k dy_1 dy_2 \delta(m_\Psi^\Psi + k \cosh y_k - m_\perp^1 \cosh y_1 - m_\perp^2 \cosh y_2)$$

$$\times \delta(k \sinh y_k - m_\perp^1 \sinh y_1 - m_\perp^2 \sinh y_2) \delta(y_1 - y_2)$$

$$= \frac{4}{\sqrt{(\mu_N^2)^2 - (\mu_D^2)^2}} \int dy_1 dy_2 \delta(y_1 - \bar{y}_c) \delta(y_2 - \bar{y}_c) \theta(\mu_N^2 - \mu_D^2), \quad (\text{A.3})$$

where $\mu_N^2 = (m_\perp^\Psi)^2 + (m_\perp^1 + m_\perp^2)^2 - k_\perp^2$, $\mu_D^2 = 2m_\perp^\Psi(m_\perp^1 + m_\perp^2)$ and $\bar{y}_c = \log\left(\mu_N^2/\mu_D^2 + \sqrt{(\mu_N^2/\mu_D^2)^2 - 1}\right)$. The integral over the transverse position variable can be computed analytically and it turns out to depend only on the variable $x = \xi/2R(\tau)$. The result of the integration is

$$Q(x) = \frac{1}{\pi R^2(\tau)} \left[1 - \frac{2}{\pi} \left(x\sqrt{1-x^2} + \arcsin x \right) \right] \theta(1-x). \quad (\text{A.4})$$

In this way the formation rate can be brought to the form

$$\begin{aligned} \lambda_F(\tau) &= \frac{1}{\tau} \int d^2k_\perp d^2q_\perp^1 d^2q_\perp^2 \frac{s(s-4m_c^2)}{\pi m_\perp^1 m_\perp^2 (s-m_\Psi^2)} \sigma_F(s) S_c(\bar{y}_c, q_\perp^1) S_c(\bar{y}_c, q_\perp^2) \\ &\times \frac{Q(x)}{\sqrt{(\mu_N^2)^2 - (\mu_D^2)^2}} \theta(\mu_N^2 - \mu_D^2). \end{aligned} \quad (\text{A.5})$$

Defining the quantity

$$K = \frac{s(s-4m_c^2)}{\pi m_\perp^1 m_\perp^2 (s-m_\Psi^2)} \frac{Q(x)}{\sqrt{(\mu_N^2)^2 - (\mu_D^2)^2}} \theta(\mu_N^2 - \mu_D^2), \quad (\text{A.6})$$

we finally arrive at the expression given in eq. (50).

If we now relax the assumption that the c quark distribution contains the factor $\delta(y_c - \eta)$, replacing it with a Gaussian $g(y_c - \eta) = (\pi\Delta y^2)^{-1/2} \exp[-(y_c - \eta)^2/\Delta y^2]$, the result of the η -integral, which is one of those to be done to obtain eq. (A.2), is

$$\int d\eta g(y_1 - \eta) g(y_2 - \eta) = (2\pi\Delta y^2)^{-1/2} \exp[-(y_c - \eta)^2/2\Delta y^2]. \quad (\text{A.7})$$

Defining $\rho = y_1 - y_2$ and $y_c = (y_1 + y_2)/2$ and expanding the l.h.s. of eq. (A.3) to order ρ^2 , we approximate the various terms typically as

$$m_\perp^1 \cosh y_1 + m_\perp^2 \cosh y_2 \simeq (m_\perp^1 + m_\perp^2) \cosh y_c (1 + \rho^2/8) \quad \text{and} \quad (\text{A.8})$$

$$m_\perp^1 \sinh y_1 + m_\perp^2 \sinh y_2 \simeq (m_\perp^1 + m_\perp^2) \sinh y_c (1 + \rho^2/8). \quad (\text{A.9})$$

We have assumed that $m_\perp^1 - m_\perp^2 \simeq 0$ for the values of q_\perp^1 and q_\perp^2 which dominate the final phase-space integration. Substituting ρ^2 with the mean value Δy^2 , the final result is reduced to the substitution

$$m_\perp^1 + m_\perp^2 \longrightarrow (m_\perp^1 + m_\perp^2) (1 + \Delta y^2/8) \quad (\text{A.10})$$

in μ_N^2 . This amounts to open up phase-space for the transverse integrations since there are more values of transverse momenta which satisfy the constraint $\theta(\mu_N^2 - \mu_D^2)$.

-
- | | |
|--|--|
| <p>[1] T. Matsui and H. Satz, Phys. Lett. B 178 (1986) 416.
 [2] G. Boyd et al., Nucl. Phys. B469 (1996) 419; F. Karsch, E. Laermann and A. Peikert, Phys. Lett. B478 (2000) 447.
 [3] F. Karsch et al., Nucl. Phys. Proc. Suppl. 94 (2001) 411.
 [4] C. Baglin <i>et al.</i> [NA38], Phys. Lett. B 220 (1989) 471 and Phys. Lett. B 255 (1991) 459.
 [5] C. Gerschel and J. Hüfner, Phys. Lett. B 207 (1988) 253; Z. Phys. C 56 (1992) 171;
 [6] M. C. Abreu <i>et al.</i> [NA50], Phys. Lett. B 410 (1997) 327.
 [7] M. C. Abreu <i>et al.</i> [NA50], Phys. Lett. B 477 (2000) 28.
 [8] J. Hüfner and B. Z. Kopeliovich, Phys. Lett. B 445 (1998) 223;</p> | <p>[9] J. Hüfner, B. Z. Kopeliovich and A. Polleri, Eur. Phys. J. A 11 (2001) 457;
 [10] B. Z. Kopeliovich and F. Niedermayer, <i>Nuclear Screening in J/ψ and Lepton Pair Production</i>, JINR-E2-84-834, unpublished.
 [11] B. Kopeliovich, A. Tarasov and J. Hüfner, Nucl. Phys. A 696 (2001) 669;
 [12] A. Capella, <i>Coherence Effects in Charmonium Production off Nuclei: Consequences for J/ψ Suppression</i>, nucl-th/0207049.
 [13] D. Kharzeev, C. Lourenco, M. Nardi and H. Satz, Z. Phys. C 74 (1997) 307;
 [14] S. Digal, P. Petreczky and H. Satz, Phys. Lett. B 514</p> |
|--|--|

- (2001) 57; Phys. Rev. D **64** (2001) 094015
- [15] C. Y. Wong, Phys. Rev. C **65** (2002) 034902
- [16] T. H. Hansson, S. H. Lee and I. Zahed, Phys. Rev. D **37** (1988) 2672.
- [17] R.A. Schneider and W. Weise, Phys. Rev. **C64** (2001) 055201.
- [18] T. Renk, R. Schneider and W. Weise, Phys. Rev. **C66** (2002) 014902
- [19] M. E. Peskin, Nucl. Phys. B **156** (1979) 365.
- [20] G. Bhanot and M. E. Peskin, Nucl. Phys. B **156** (1979) 391.
- [21] P. Braun-Munzinger and J. Stachel, Phys. Lett. B **490** (2000) 196;
- [22] R. L. Thews, M. Schroedter and J. Rafelski, Phys. Rev. C **63** (2001) 054905; R. L. Thews, *Nonlinear Behavior of Quarkonium Formation and Deconfinement Signals*, hep-ph/0206179.
- [23] L. Grandchamp and R. Rapp, Phys. Lett. B **523** (2001) 60; Nucl. Phys. A **709** (2002) 415;
- [24] M. I. Gorenstein *et al.*, Phys. Lett. B **524** (2002) 265;
- [25] R. K. Ellis, FERMILAB-CONF-89-168-T *Lectures given at 17th SLAC Summer Inst., Stanford, CA, Jul 10-21, 1989*;
- [26] R. V. Gavai *et al.*, Int. J. Mod. Phys. A **10** (1995) 2999;
- [27] M. Gluck, E. Reya and A. Vogt, Z. Phys. C **67** (1995) 433;
- [28] B. Z. Kopeliovich and A. V. Tarasov, Nucl. Phys. A **710** (2002) 180;
- [29] G. A. Schuler, *Quarkonium Production and Decays*, hep-ph/9403387;
- [30] R. Vogt, Phys. Rept. **310** (1999) 197.
- [31] J. L. Nagle [PHENIX], *Leptonic Observables in Ultra-Relativistic Heavy Ion Collisions*, nucl-ex/0209015.
- [32] C. Zhai and B. Kastening, Phys. Rev. **D52** (1995) 7232.
- [33] P. Aurenche, F. Gelis, H. Zaraket and R. Kobes Phys. Rev. **D58** (1998) 085003; P. Aurenche, F. Gelis and H. Zaraket, Phys. Rev. **D61** (2000) 116001.
- [34] M. Le Bellac, *Thermal Field Theory*, Cambridge University Press, Cambridge, 1996;
- [35] A. Peshier, B. Kämpfer and G. Soff, Phys. Rev. **C61** (2000) 045203; P. Levai and U. Heinz, Phys. Rev. **C57** (1998) 1879.
- [36] B. Tomasik, U. A. Wiedemann and U. W. Heinz, nucl-th/9907096.
- [37] K. Adcox *et al.* [PHENIX], Phys. Rev. Lett. **88** (2002) 192302.
- [38] Y. Oh, S. Kim and S. H. Lee, Phys. Rev. C **65** (2002) 067901;
- [39] X. N. Wang and F. Yuan, Phys. Lett. B **540** (2002) 62;
- [40] K. Martins, D. Blaschke and E. Quack, Phys. Rev. C **51** (1995) 2723;
- [41] C. Y. Wong, E. S. Swanson and T. Barnes, Phys. Rev. C **62** (2000) 045201; C **65** (2002) 014903;
- [42] G. R. Burau, D. B. Blaschke and Y. L. Kalinovsky, Phys. Lett. B **506** (2001) 297;
- [43] A. Polleri, *Bound State Kinetics in High-Energy Nuclear Collisions*, nucl-th/0303065;
- [44] J. P. Blaizot and J. Y. Ollitrault, Phys. Rev. D **39** (1989) 232.
- [45] X. M. Xu, D. Kharzeev, H. Satz and X. N. Wang, Phys. Rev. C **53** (1996) 3051;
- [46] F. Cooper and G. Frye, Phys. Rev. D **10** (1974) 186;
- [47] A. Capella, E. G. Ferreira and A. B. Kaidalov, Phys. Rev. Lett. **85** (2000) 2080; J. P. Blaizot, P.M. Dinh and J. Y. Ollitrault, Phys. Rev. Lett. **85** (2000) 4012; J. Hüfner, B. Z. Kopeliovich and A. Polleri, *Fluctuations of the Transverse Energy in Pb+Pb Collisions and J/ψ Suppression*, nucl-th/0012003.
- [48] N. Armesto and A. Capella, Phys. Lett. B **430** (1998) 23; N. Armesto, A. Capella and E. G. Ferreira, Phys. Rev. C **59** (1999) 395;
- [49] A. Capella, U. Sukhatme, C. I. Tan and J. Tran Thanh Van, Phys. Rept. **236** (1994) 225.